A realistic energy optimization model for smart-home appliances*

Michael David de Souza Dutra†, Miguel F. Anjos‡§, Sébastien Le Digabel¶

January 25, 2019

Abstract

Smart homes have the potential to achieve optimal energy consumption with appropriate scheduling. The control of smart appliances can be based on optimization models, which should be realistic and efficient. However, increased realism also implies an increase in solution time. Many of the optimization models in the literature have limitations on the types of appliances considered and/or their reliability. This paper proposes a home energy management scheduling model that is more realistic and efficient. We develop a mixed integer linear optimization model that minimizes the energy cost while maintaining a given level of user comfort. Our main contribution is the variety of specific appliance models considered and their integration into a single model. We consider the use of energy in appliances and electric vehicles (EVs) and take into account renewable local generation, batteries, and demand-response. Our models of a shower, a fridge, and a hybrid EV consider both the electricity consumption and the conventional fuel cost. We present computational results to validate the model and indicate how it overcomes the limitations of other models. Our results, compared to the best competitors, provide cost savings ranging from 8% to 389% over a horizon of 24 hours.

Keywords: Smart home, Energy management system, Power demand, Residential load, Multi-class appliance.

1 Introduction and Related Work

In 2006, the European Technology Platform Smart Grid defined a smart grid to be "an electricity network integrating users, consumers, and generators in order to produce and deliver economic, secure and sustainable electricity supplies". Smart grids are used worldwide [31, 35], and many distribution companies use demand-response pricing mechanisms in the residential sector.

A smart home is a home where the appliances and devices can be controlled remotely, and the number of such homes has increased considerably in recent years. In North America the number is expected to reach 46.2M by 2020 [44], corresponding to 35% of households. In Europe, 44.9M are expected by 2020, corresponding to 20% of households. Governments are supportive because smart homes allow investment in the grid infrastructure to be postponed. Moreover, if the local generation comes from renewables, the environmental impact of coal/oil-based generation is reduced. The advantage for the users are that they can optimize energy usage to reduce costs while maintaining a desired comfort level; sell electricity back to the utility; or obtain financial incentives from demand-response programs.

We define smart home components (SHCs) to be the appliances, machines, and technologies available for use in smart homes. Examples of SHCs include photovoltaic solar panels (PVs), wind turbines (WTs), combined heating power (CHP), energy storage systems (ESSs), heating, ventilation, and air-conditioning (HVAC), and water heating (WH). SHCs are controlled by a home energy management system (HEMS), which also respects the power capacity (maximum amount of electric power that the house can use at any given time), ensures an adequate level for the air/water temperature, and makes decisions about when to buy and sell electricity. In essence, the HEMS solves a scheduling problem; for more details see [92].

See [72] and [12] for surveys of modeling approaches for this scheduling problem. However, existing models for appliance scheduling [49, 71] often do not accurately account for the operational and energy-consumption characteristics of each device. Table 1 summarizes the EMS models in the literature: columns 2 to 16 indicate the features included. The column *IBR constraints* indicates the use of inclining blocking rates (IBR), a pricing scheme where the prices increase for each incremental block of consumption. The column *Fraction of step* indicates that the appliances can be used for brief cycles. This occurs when,

*GERAD and Département de mathématiques et génie industriel, Polytechnique Montréal, C.P. 6079, Succ. Centre-ville, Montreal, Quebec, Canada H3C 3A7.

†michaeldavid.dutra@polymtl.ca

‡anjos@stanfordalumni.org

§School of Mathematics, University of Edinburgh, Edinburgh EH9 3FD, United Kingdom

¶sebastien.le.digabel@gerad.ca

for example, a model uses a fixed interval of 10 min but allows the A/C to operate in cycles of 2.5 min. The column *Comfort* indicates the model used for the comfort function, and *Pricing* indicates the pricing policy, where TOU is time-of-use and RTP is real-time pricing. Finally, the column *Objective* indicates the optimization objective(s).

Table 1 shows that no article uses a detailed model for every appliance. Detailed appliance models give more accurate information and can better predict consumption, which is important for the evaluation of expansion strategies in the medium- and long-term [54]. Such models are available in the literature: see [43] for electric vehicles (EVs), [91] for PV, and [1] for PV/EV. However, the resulting optimization models may be computationally expensive to solve. Several authors [24, 55, 36] have emphasized the importance of a realistic model for the controllable appliances and the need for a trade-off between realism and computational difficulty. Realistic approaches to smart home scheduling require appropriate appliance models [55], and this is the motivation for this paper. Our specific goal is to create a realistic optimization model that can be solved in a reasonable time. Our main contribution is that we combine all of the SHCs of Table 1 into a single HEMS, formulated as a mixed integer linear optimization problem. In summary, we develop a model that finds the optimal cost while maintaining a high level of user comfort. The secondary contributions are:

1. Fridge model: We develop a realistic fridge model by linearizing a nonlinear model.
2. Shower model: In some countries, such as Brazil, the electric shower is one of the largest components of the electricity bill.
3. New EV model: To the best of our knowledge, no previous work has considered the additional costs of fuel or recharging outside the house.

This paper is organized as follows. In Section 2, we introduce the appliance models, IBR pricing, thermal machines, and other components. Section 3 describes our instances, and Section 4 presents the results. Section 5 provides concluding remarks.

2 Mathematical Models

In this section, we describe the models for the SHCs and the integrated optimization model. We consider only power consumption, and we retain the units used by the corresponding references. The nomenclature is provided before references.

2.1 Photovoltaic solar panels (PV) and Solar Collector Models

The PV and solar collector models calculate the values of the parameters E^t_{pv} and T^t_{in}. We first need to estimate T^t_o so that we can use the formulas from [5, Example 9, Section 14.12]. We also need to know the quantity of solar radiation available at the surfaces of the panels and collectors. We used the equations from [30, Chapters 1 and 2] (without shading and "track moving" but with "clear sky"). We implemented four models: the isotropic diffuse model, the HDRK model, the Perez model, and the ASHRAE revised clear sky model (Tau Model) from [5, Chapter 14] and [6, Chapter 35]. From these we selected the Perez model. We also considered the absorptance effect.

We must convert the solar radiation into power for the PV and heat for the solar collector. For the PV, we use the approach from [61] with $V = V_{mp}$; we replace Equation 3 of [61] by Equation 9 of [25]. For the cell temperature, we use the approach from [30, Section 23.3]. For the solar collector, we use the collector-efficiency equations from [30, Chapters 3–6] with the factor F' = 0.8, the temperature of the plates equal to the outside temperature, and the difference of temperature between the plates and glass set to 20^{o}C. All the layers of glass have the same temperature, and the inlet water comes from the street.

2.2 Wind Turbines (WT) Model

The WT model forecasts the value of E^t_{wt}. Villaneuva & Feijóo [85] propose a relationship between wind speed and WT power produced. They consider operation at maximum capacity and specify cut-in and cut-out inequalities:

$$\begin{array}{cc} \text{Wind speed interval (m/s)} & \text{Output power (W)} \\ U < U_{CutIn} & 0 \\ U_{CutIn} \leq U < U_{Pmax} & 0.5A\rho U^3 C_{p2} \\ U_{Pmax} \leq U \leq U_{CutOut} & Pmax \\ U > U_{CutOut} & 0 \end{array} \tag{1}$$

where U is the wind speed (m/s); U_{CutIn} is the lowest wind speed (m/s) at which it is possible to obtain power from the wind; U_{Pmax} is the wind turbine power speed rate (m/s); A is the area of the air-stream, measured in a perpendicular plane to the direction of the wind speed (m^2); ρ is the air density (kg.m^{-3}); C_{p2}

Table 1: Summary of features of EMS models

Reference	WT	PV	Solar Collector	ESS	WH	Shower	Freezer/Fridge	HVAC	Phase Machines	A_{IEUI}	EV	CHP	Lighting	IBR Constraints	Fraction of Step	Comfort	Pricing	Objective
Our model	x	x	x	x	x	x	x	x	x	x	x	x		x	x	L	TOU	$\downarrow$ D vs C
[79]	x	x						x			x	x					NC	$\downarrow$ C
[46]									x	x				x		NL	RTP	many
[89]								x							x	Q	NC	$\downarrow$ TD
[88]													x			L		$\downarrow$ IL
[87]				x					x	x						Q	NC	$\downarrow$ C vs D vs B
[26]								x	x	x						Q	DA RTP	$\downarrow$ D vs C
[47]									x	x							DA RTP	$\downarrow$ C
[29]					x											L	DA TOU	$\downarrow$ B
[41]								x								L	DA NC	$\downarrow$ B vs D
[67]									x	x						CF	NC RTP	$\uparrow$ -D vs C
[42]				x				x	x	x		x				L	DA NC	$\downarrow$ C
[94]									x	x				x		L	NC	$\downarrow$ C vs W
[10]	x	x		x												L		$\downarrow$ C
[64]					x			x								L	NC	$\uparrow$ -D vs C
[65]					x			x								L	NC	$\uparrow$ -D vs C
[56]									x	x				x		L	RTP	$\downarrow$ C vs W
[34]									x	x							RTP, TOU	$\downarrow$ C
[68]				x						x	x					L	TOU	$\downarrow$ C / $\downarrow$ C vs D
[19]				x										x			NC	$\downarrow$ C
[38]										x							DA TOU	$\downarrow$ C
[2]									x	x						L	NC	$\downarrow$ C / $\downarrow$ C vs PL
[3]				x					x	x							DA RTP	$\downarrow$ C
[8]	x	x		x	x			x	x	x		x				NL	RTP	many
[9]				x	x			x	x	x		x				NL	RTP	many
[4]				x				x	x	x						L	NC	$\downarrow$ C vs D
[20]					x			x	x	x	x						RTP	$\downarrow$ B
[93]				x	x			x		x	x						RTP	$\downarrow$ C
[86]					x					x							NC	$\downarrow$ C
[60]			x		x			x	x	x	x					L	RTP	$\downarrow$ C
[70]					x		x	x									TOU	$\downarrow$ C
[18]								x	x	x						L	NC	$\downarrow$ C
[71]					x		x	x		x						NL	TOU	$\uparrow$ -D vs C
[52]		x		x							x							$\downarrow$ C
[57]		x		x													Flat	$\downarrow$ C vs CO_2
[83]		x		x							x							$\downarrow$ E[C]
[37]		x		x						x	x							$\downarrow$ C
[78]	x			x					x	x						L	RTP	$\downarrow$ C
[36]		x		x	x						x			x		–	TOU,RTP	$\downarrow$ C
[74]		x		x			x	x									TOU	$\downarrow$ C vs D
[55]		x		x					x	x	x						NC	$\downarrow$ C
[73]	x	x		x				x		x	x						NC	$\uparrow$ Profit
[58]				x				x		x							NC	$\downarrow$ C
[33]		x		x							x						NC	$\downarrow$ C
[63]		x		x	x			x	x		x						NC	$\downarrow$ C
[77]	x	x		x	x		x	x		x		x	x			L	RTP	$\downarrow$ C
[76]	x	x		x	x		x	x		x		x	x			L	RTP	$\downarrow$ C / $\downarrow$ C vs PL
[48]				x	x		x	x		x	x	x					TOU	$\downarrow$ C

Legend: $\downarrow$: Minimize $\uparrow$: Maximize IL: Illumination level D: Discomfort -D: Comfort C: Cost L: Linear Q: Quadratic NC: Not constant TD: Thermal discomfort B: Electricity bill BL: Battery loss DA: Day ahead CF: concave function W: Waiting time NL: Nonlinear PL: Peak load

is the power coefficient, which is the ratio between the power produced by the WT and the power carried by the free air-stream; U_{CutOut} is the upper limit (m/s) at which it is possible to get power from the wind; and $Pmax$ is the rated power (W).

We can find ρ using the ideal gas law for dry air, Equation 1.18 from [82].

2.3 Heating, Ventilation, and Air Conditioning (HVAC) Model

The HVAC model is outlined in this subsection. We discuss also assumptions and flexibility strategies. With $\Upsilon = \Delta t_2 / V_{house}\rho_{air}c_{air}$, the HVAC model is

$$T^{t+1}_{room} = T^t_{room} + \Upsilon[3600(P_{heating}z^t_{HVAC} - P_{cool}z^t_{air})] + \Upsilon(G^t) \ \forall \ t \in T\backslash\{|T|\} \tag{2}$$

$$G^t = \left[\frac{A_{ceiling}}{R_{ceiling}} + \frac{A_{wall}}{R_{wall}} + \frac{A_{window}}{R_{window}}\right](T^t_o - T^t_{room}) + [n_{ac}V_{house}\rho_{air}c_{air}](T^t_o - T^t_{room}) + 3600H^t_p + 3600(SHGC)A_{window}H^t_{sun} \ \forall \ t \in T\backslash\{|T|\} \tag{3}$$

$$T^1_{room} = T^1_o \tag{4}$$
$$x^t_{HVAC} = P_{heating}z^t_{HVAC} + P_{cool}z^t_{air} \ \forall \ t \in T$$

$$\begin{aligned} y^t_{HVAC} &\in \{0,1\} \ \forall \ t \in T \\ y^t_{air} &\in \{0,1\} \ \forall \ t \in T \\ 1 &\geq y^t_{HVAC} + y^t_{air} \ \forall \ t \in T \end{aligned} \tag{5}$$

$$\begin{aligned} z^t_{HVAC} &\leq y^t_{HVAC} \ \forall \ t \in T \\ z^t_{air} &\leq y^t_{air} \ \forall \ t \in T \end{aligned} \tag{6}$$

$$\begin{aligned} z^t_{HVAC} &\geq 0 \ \forall \ t \in T \\ z^t_{air} &\geq 0 \ \forall \ t \in T \end{aligned} \tag{7}$$

$$\begin{aligned} V^t_{HVAC} &\geq T^t_{room} - T^t_f \ \forall \ t \in D_{air} \\ V^t_{HVAC} &\geq -T^t_{room} + T^t_f \ \forall \ t \in D_{air} \end{aligned} \tag{8}$$

Constraints (2) to (7) represent the room temperature, and (8) permit deviation from the target temperature and measure the discomfort during the intervals when HVAC is used. Constraints (2) and (3) are based on Shao et al. [75]. They propose a model with a 1.2% total daily energy difference. The differences between our model and their model are explained below.

Assumptions: A_{wall} in [75] is derived from the floor area, assuming that the height of the house is 10 ft. If A_{wall} is not given by the user, we assume that the floor is square and calculate A_{wall} accordingly. In [75] the authors consider a specific window turned to the south. In our model, we consider every window of the same type. The values for H^t_p, SHCG, and n_{ac} are not available in [75]. H_p can be found ([8], [90, pp. 41–43]) via $H_p = P_{activity}A_{body}$, where $P_{activity}$ is the metabolic rate and $A_{body} = 0.202m^{0.425}h^{0.725}$, where h is the height (m) and m is the mass of the body (kg). We define np^t to be the number of occupants at time t. We then have $H^t_p = \sum_{i=1}^{np^t} P^t_{activity,i}A^t_{body,i} \ \forall \ t \in T$.

For SHCG, we used the average of the values of [5, p. 353], and H_{solar} is calculated from our PV model. We have $\rho C_{air} = \frac{1214.4J}{^oC\times m^3} \approx \frac{0.018Btu}{^oF\times ft^3}$ from [5, Chapter 17]: $n_{ac} = ACH = 3.6Q_i/V$, $Q_i = A_L IDF$, $A_L = A_{es}A_{ul}$, where ACH is the hourly air change; Q_i is the infiltration airflow rate (L/s); V is the building volume (m^3); A_L is the effective leakage area (cm^2) (including the flue) at a reference pressure difference of 4 Pa, assuming a discharge coefficient CD of 1; IDF is the infiltration driving force ($L/(s.cm^2)$); A_{es} is the exposed surface area of the building (m^2); and A_{ul} is the unit leakage area (cm^2/m^2). This gives $ACH = 3.6A_{es}A_{ul}IDF/V$. With the values given for IDF [5, Table 5 of Chapter 17] and A_{ul} [5, Table 3 of Chapter 17], n_{ac} has an acceptable value.

Our other assumptions are as follows: i) there is a single conditioned space; ii) no independent thermal storage is linked to the main HVAC equipment; iii) the humidity control is neglected; iv) the internal heat sources of the equipment are neglected; v) the temperature is constant throughout the space.

We have rewritten the model from [75] given the considerations above to arrive at an on-off model composed of Constraints (2) to (5), (8).

Flexibility: (2) introduces the on-off feature, since y^t_{HVAC} and y^t_{air} are binary variables. Thus, we are working with fixed power in a fixed time interval. However, forcing a machine to operate for a full interval could generate an overcharge. Let the variable z^t_a be the fraction of Δt during which appliance a is on. We have $z^t_a y^t_a = z^t_a$. We can model the implications with inequalities such as (6). Therefore, with the new

variable, we can build a single model that is represented by Constraints (2) to (8). With the objective function (76), we can, without any impact on the results, drop the variables y^t_{HVAC} and y^t_{air} and the restrictions (5) to (6). We refer to this as the *Fraction of step*.

The strategy above does not indicate when the machine is on/off in the fixed time interval. Given x^t_{HVAC} for each $t \in T$, we can find whether the machine is on or off at each second.

The temperature at the end of the period depends on exactly when it is used. If it is used at the end of the period, the results are closer to the results for the complete optimization model. However, the difference is not as large. With nomimal power of 25 kW, the difference in temperature will be around 0.12^oC at some point in the time interval.

Note that the addition of z^t_a does not violate energy conservation. For example, suppose an appliance has a power of 5000 W and it operates for 50% of the time, giving a consumption of $5000\,W \times 0.5\Delta t$. It will contribute $2500\,W \times \Delta t$ to the conservation constraint.

2.4 Water Heaters (WH) Model

The Water Heaters model is outlined in this subsection. A comparison with reference model is done for validation purposes. With $\Psi = \Delta t_2/(v_{tank}C_p)$, the HVAC model is

$$T^{t+1}_{out,wh} = T^t_{out,wh} + \Psi[-227.4 fr^t_{wh} C_p (T^t_{out,wh} - T^t_{in})] + \Psi[3600(x^t_{wh} + 1000 P^t_{CHPt})] - \Psi[3600(UA)_{wh}(T^t_{out,wh} - T^t_{room})] \;\forall\, t \in T\backslash\{|T|\} \quad (9)$$

$$T^1_{out,wh} = T^1_{in} \quad (10)$$
$$x^t_{wh} = P_{wh} y^t_{wh} \;\forall\, t \in T$$

$$y^t_{wh} \in \{0,1\} \;\forall\, t \in T \quad (11)$$

$$V^t_{wh} \geq T^{wh}_f - T^t_{out,wh} \;\forall\, t \in D_{wh} \quad (12)$$
$$V^t_{wh} \geq -T^{wh}_f + T^t_{out,wh} \;\forall\, t \in D_{wh}$$

$$y^t_{wh} \leq E_{wh} \;\forall\, t \in T \quad (13)$$

Constraints (9) to (11) represent the WH temperature, and (12) permit deviation from the target temperature and measure the discomfort during the intervals when hot water is used. If $E_{wh} = 0$, there is no WH, and $T^t_{out,wh}$ is at most the street water temperature or the water temperature from SC if it exists. In this case, we need Constraint (13), which also imposes an upper bound on the temperature. Note that T^t_{room} in (9) comes from the HVAC model.

We assume that all the water inside the WH is at the same temperature. The model was constructed from [30, Equation 8.3.3] and validated by comparisons with the model from [75], which was validated experimentally.

For a validation example, we convert units where necessary and use the following data: the room temperature is given in Figure 1, $T^1_{out,wh} = 77^oF$, $x^t_{wh} = 5\,\text{kW}\;\forall\, t \in T$, the surface area of the WH equals $5\,\text{ft}^2$, the tank heat resistance equals $25^oF \cdot ft^2 \cdot h/Btu$, $\Delta t = 10\,\text{min}$, $T^t_{in} = 104^oF\;\forall\, t \in T$, $v_{tank} = 80\,\text{gallons}$, $fr^t_{wh} = \ddot{f}\;\forall\, t \in T\,(\text{gallons/min})$ for $\ddot{f} \in \{0,1,5,10\}\;\forall\, i$. If we assume that the WH is always on, we obtain the results of [75] when $fr^t_{wh} > 0\;\forall\, t \in T$, as shown in Figures 2 and 3. When $fr^t_{wh} = 0\;\forall\, t \in T$, the model deviates after about 150^oC, but in practice there are mechanisms to avoid water evaporation. Thus, our model is faithful to the results of [75].

2.5 Shower Model

In this subsection, the shower model is outlined and thermodynamics explanations are given. The shower is modeled by:

$$T^t_{chu\_hand} \leq T^t_{out,wh} \;\forall\, t \in D_{chu} \quad (14)$$
$$T^t_{chu\_hand} \geq T^t_{inlet} \;\forall\, t \in D_{chu}$$

$$T^t_{out,chu} = T^t_{chu\_hand} + 60 x^t_{chu}/(C_e fr^t_{chu}) \;\forall\, t \in D_{chu} \quad (15)$$
$$x^t_{chu} = P_{chu} y^t_{chu,hot} \;\forall\, t \in D_{chu}$$

$$x^t_{chu} = 0 \;\forall\, t \notin D_{chu} \quad (16)$$

$$V^t_{chu} \geq T^{chu}_f - T^t_{out,chu} \;\forall\, t \in D_{chu} \quad (17)$$
$$V^t_{chu} \geq -T^{chu}_f + T^t_{out,chu} \;\forall\, t \in D_{chu}$$

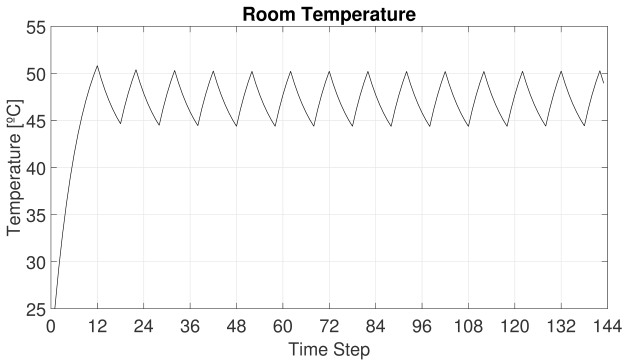

Figure 1: Room temperature for validation example.

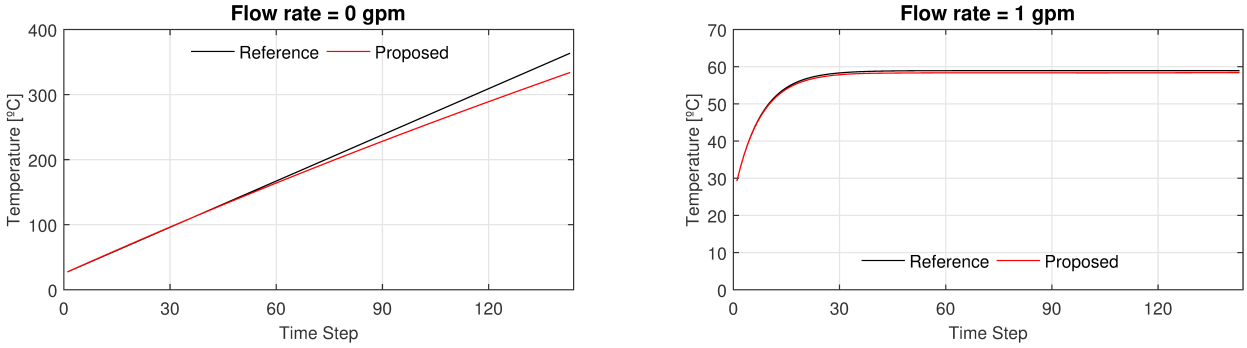

Figure 2: Comparison of our model and reference model from [75]: WH always on and low flow rate.

$$y^t_{chu,hot} \in \{0,1\} \ \forall \ t \in D_{chu} \tag{18}$$

Constraints (14) place bounds on the shower temperature without using the shower resistance. Constraints (15) to (16) represent the shower temperature, and (17) permit deviation from the target temperature and measure the discomfort during the intervals when the shower is used. Constraints (18) are the binary restrictions.

We obtain Constraints (14) to (18) from [90, Chapter 1] through the thermodynamics formula $\dot{Q} = \dot{m}C_p\Delta T$ where $\dot{m}$ is the mass flow rate of a fluid flowing in a pipe (kg/s); C_p is the specific heat of the fluid (J/kg·^oC); ΔT is the temperature difference (^oC); and $\dot{Q}$ is the rate of net heat transfer of the control volume (W). Moreover, $\dot{m} = \rho V A_c$ where ρ is the fluid density; V is the average fluid velocity in the flow direction; and A_c is the duct cross-sectional area. This gives $\dot{Q} = \rho\dot{V}C_p\Delta T$, where $\dot{V}$ is the volumetric flow rate (m^3/s). We write $P = \rho\dot{V}C_p\Delta T$ where P is the power (W) lost or injected.

For each step $t \in D_{chu}$, $P_{chu} = P$, f_r is the equivalent measure of $\dot{V}$ (gpm) and $\Delta T = T_{out,chu} - T_{chu\_hand}$. This gives (15).

2.6 Batteries (ESS) Model

The ESS model is outlined in this subsection. A comparison with reference models is done to demonstrate our differences. The ESS is modeled by

$$SOC^{t+1} = SOC^t + \frac{100\Delta t_2}{E_{bat}}\left(P^{ch,t}_{bat}\eta^{ch}\mu - \frac{P^{dch,t}_{bat}}{\eta^{dch}\mu} - p_{loss}y^t_{float}\right) \ \forall \ t \in T\backslash\{|T|\} \tag{19}$$

$$SOC^t \geq SOC_{min} \ \forall \ t \in T \tag{20}$$

$$SOC^t \leq SOC_{max} + (100 - SOC_{max})y^t_{float} \ \forall \ t \in T \tag{21}$$

$$SOC^1 = SOC_{min} \tag{22}$$

$$\begin{aligned} P^{ch,t}_{bat} &\leq \tfrac{P^{ch}_{max}}{\eta^{ch}\mu}y^{ch,t}_{bat} \ \forall \ t \in T \\ P^{ch,t}_{bat} &\geq \tfrac{P^{ch}_{min}}{\eta^{ch}\mu}y^{ch,t}_{bat} \ \forall \ t \in T \\ P^{dch,t}_{bat} &\leq P^{dch}_{max}\eta^{dch}\mu y^{dch,t}_{bat} \ \forall \ t \in T \\ P^{dch,t}_{bat} &\geq P^{dch}_{min}\eta^{dch}\mu y^{dch,t}_{bat} \ \forall \ t \in T \end{aligned} \tag{23}$$

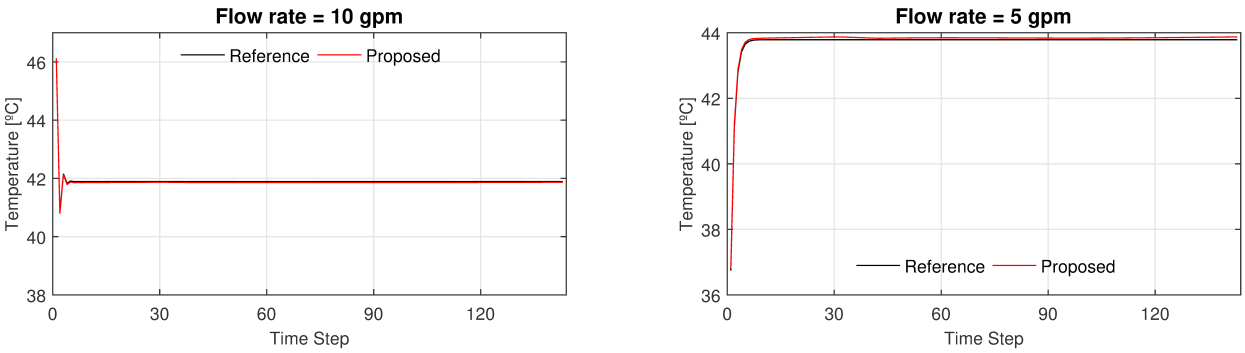

Figure 3: Comparison of our model and reference model from [75]: WH always on and high flow rate.

$$1 \geq y_{bat}^{dch,t} + y_{bat}^{ch,t} \ \forall \ t \in T \tag{24}$$

$$\begin{aligned} y_{bat}^{dch,t} &\in \{0,1\} \ \forall \ t \in T \\ y_{bat}^{ch,t} &\in \{0,1\} \ \forall \ t \in T \\ y_{float}^{t} &\geq 0 \ \forall \ t \in T \end{aligned} \tag{25}$$

Constraints (19) establish the relationships between the state of charge (SOC), discharging and charging powers, and battery float losses. Constraints (20) place a lower bound on the SOC. Constraints (21) place an upper bound on the float losses that is activated when a threshold is reached. Constraint (22) sets an initial value for the SOC. Constraints (23) set bounds on the discharging and charging power. Constraints (24) ensure that at each $t \in T$ the battery either charges or discharges. Constraints (25) are the domain restrictions.

We based our model on [8], [9], and [93]. The differences between these models will be explained using the following data: $|T| = 144$, $E_{bat} = 24\,\text{kWh}$, $SOC_{max} = 80\%$, $SOC_{min} = 20\%$, $P_{max}^{ch} = P_{max}^{dch} = 3.3\,\text{kW}$, $P_{min}^{ch} = P_{min}^{dch} = 0.3\,\text{kW}$, $\eta^{ch} = \eta^{dch} = 0.91$, and $\mu = 1$. We define the objective function as $\max 30SOC^2 - \sum_{t \in T} SOC^t$. Thus, in Interval 1, the battery will charge at a maximal power and in Interval 2 it will discharge at a maximal power.

The solution to the models of [8] and [9] is $SOC^2 = 22.0854$, $SOC^t = 20 \ \forall \ t \in T \backslash \{2\}$, $P_{batt}^{ch,1} = P_{batt}^{dch,2} = 3.003$, and the other power variables are null. Thus, the charging consumption was 3.003 KW instead of 3.3 KW. For the discharging, $P_{batt}^{dch,2}$ takes the value of the power inside the battery instead of the power sent to the house. Thus, when we put these variables into the energy conservation constraints, they use different values than the values sent to or consumed in the battery model. Therefore, there is an energy construction if we take the home as the reference point.

The model from [93] gives the same objective value, but we could have maximal power charging in the battery.

Constraints (21) implement the battery float charge loss, which results from the energy used to maintain the battery charge when SOC $\approx 100\%$ [16].

2.7 Fridge Model

The fridge model is outlined in this subsection. A comparison with reference model is done for validation purposes. The fridge is modeled by

$$\begin{aligned} T_{freezer}^{t+1} &= T_{freezer}^{t} - (7/25)\Delta t y_{comp}^{t} + (15/67)\Delta t \left(1 - y_{comp}^{t}\right) \ \forall \ t \in T \backslash \{|T|\} \\ T_{refri}^{t+1} &= T_{refri}^{t} - 0.1467\Delta t y_{comp}^{t} + 0.1196\Delta t (1 - y_{comp}^{t}) \ \forall \ t \in T \backslash \{|T|\} \end{aligned} \tag{26}$$

$$T_{freezer}^{1} = T_{freezer}^{start} \tag{27}$$

$$T_{refri}^{1} = T_{refri}^{start} \tag{28}$$

$$x_{refri}^{t} = P_{comp} y_{comp}^{t} \ \forall \ t \in T \tag{29}$$

$$\begin{aligned} V_{freezer}^{t} &\geq T_{f}^{freezer} - T_{freezer}^{t} \ \forall \ t \in T \\ V_{freezer}^{t} &\geq 0 \ \forall \ t \in T \\ V_{refri}^{t} &\geq T_{f}^{refri} - T_{refri}^{t} \ \forall \ t \in T \\ V_{refri}^{t} &\geq 0 \ \forall \ t \in T \end{aligned} \tag{30}$$

$$y_{comp}^{t} \in \{0,1\} \ \forall \ t \in T \tag{31}$$

We consider a frost-free top-mount refrigerator. Constraints (26) represent the freezer temperature and fridge temperature, respectively. Constraint (27) establishes the initial freezer temperature, and Constraint (28) establishes the initial fridge temperature. Constraints (29) initialize the x^t_{refri} values for the link with the complete model. Constraints (30) permit deviation from the target temperature and measure the discomfort, and Constraints (31) are the binary restrictions.

A transient model has been developed [14, 13] for the temperatures of refrigerated compartments; the predicted energy consumption has a maximum deviation of ±2%. Our model is based on this, with some adjustments. We observe a correlation between the power consumption and the air temperature at the evaporator outlet [13, Figures 2.15 and 2.16]. We apply Newton's law of cooling to find the temperature at the evaporator outlet when the compressor is operating. When it is off, we have a choice of two approaches. In the first, suggested by the author of [14] via email, we assume that the temperature at the evaporator outlet is the same as the air temperature at the evaporator inlet. In the second, we use Newton's law of cooling for the temperature increase around the evaporator outlet. We selected approach 2.

We can rewrite Equation 3.71 from [13] as $(T^t_{o,e})' = T^t_{o,e} + (3600 w_{fan})/(\dot{m}_a C_{p,a}) y^t_{comp}$, where $(T^t_{o,e})'$ is the air temperature of the fan discharge (^oC); w_{fan} is the rated fan power (W); $\dot{m}_a$ is the total mass flow rate of air (kg/h); and $C_{p,a}$ is the specific heat at a constant pressure (J/kg^oC). The fan is on only when the compressor is on.

With $\kappa \in \{T_{newton_2}, rT^{t-1}_{freezer} + (1-r)T^{t-1}_{refri}\}$ and following [13], we obtain $\forall\, t \in T\backslash\{|T|\},\ \forall * \in \{r, f\}$: $T^{t+1}_* = T^t_{eq,*} - (T^t_{eq,*} - T^t_*)\exp\left(-\frac{60\Delta t\left(Ua_* + UA_m + \frac{\dot{m}_* C_{air}}{3600} y^t_{comp}\right)}{C_*}\right)$ where $T^t_{eq,f}$ ($T^t_{eq,r}$) is associated with the steady-state temperature of the freezer (fridge) if constant conditions are maintained at time t (^oC); UA_f (UA_r) is the global freezer (fridge) thermal conductance (W/^oC); $\dot{m}_{d,f}$ ($\dot{m}_{d,r}$) is the air flow leaving the freezer (fridge) when the door is open; T^t_a is the exterior temperature around the fridge at time t (^oC); UA_m is the global mullion thermal conductance (W/^oC); $T^t_f = T^t_{freezer}\ \forall\, t \in T$; and $T^t_r = T^t_{refri}\ \forall\, t \in T$. Note that T^t_a is T^t_{room} from the HVAC model.

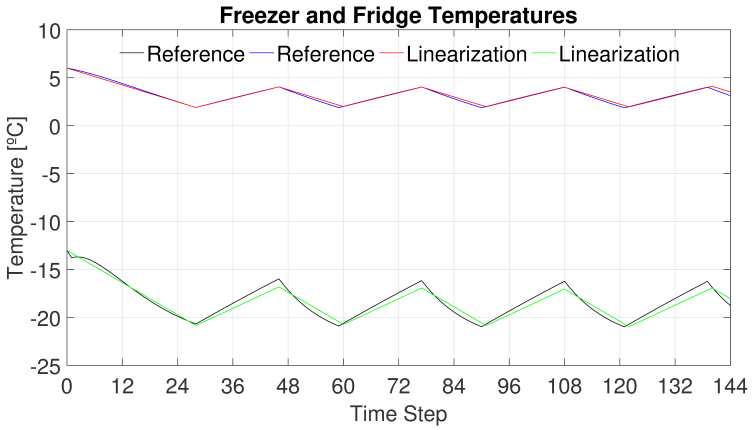

Figure 4: Comparison of simulation results for fridge from linearization and reference model.

To simplify this nonlinear model, we perform a linear regression, obtaining: $T^{t+1}_f = T^t_f - (7/25)\Delta t y^t_{comp} + (15/67)\Delta t(1 - y^t_{comp})$ for the freezer and $T^{t+1}_r = T^t_r - 3.5/25\Delta t y^t_{comp} + 7.25/67\Delta t(1 - y^t_{comp})$ for the fridge. Figure 4 presents simulation results for the linearizations, and they agree well with the reference model [13]. We thus obtain (26) to (31).

2.8 Plug-in Hybrid Electric Vehicle (EV) Model

In this subsection, the EV model is outlined. We explain also considerations used in the formulation. Let ϱ^t be the vector $\left(y^{dch,t}_{EVbat}, y^{ch,t}_{EVbat}, y^t_{EV\,float}\right)\ \forall\, t \in T$. The EV is modeled by

$$\begin{aligned} EVSOC^{t+1} &= EVSOC^t + \tfrac{100\Delta t_2}{EEV_{bat}}\left(P^{ch,t}_{EVbat}\eta^{ch}_{Ev}\mu_{Ev} - \tfrac{P^{dch,t}_{EVbat}}{\eta^{dch}_{Ev}\mu_{Ev}} - EVp_{loss}y^t_{EV\,float}\right) \\ &\forall\, t \in T\backslash\{|T|\}, s \in \{1,2,\ldots,n_{trips}\} : t^s_{start} \le i < t^s_{end}, t^1_{start} \le t < t^1_{end} \end{aligned} \tag{32}$$

$$\begin{aligned} EVSOC^{t+1} &= EVSOC^t + \tfrac{100\Delta t}{EEV_{bat}}\left(P^{ch,t}_{EVbat}\eta^{ch}_{Ev}\mu_{Ev} - \tfrac{P^{dch,t}_{EVbat}}{\eta^{dch}_{Ev}\mu_{Ev}} - EVp_{loss}y^t_{EV\,float}\right) \\ \forall\, s \in \{1,2,\ldots,n_{trips}\}, t \in \left\{1,2,\ldots,t^1_{end}-1\right\} &\cup \left\{t^s_{start}, t^s_{start}+1, \ldots, t^{s+1}_{end}-1\right\} : t^1_{start} > t^1_{end} \end{aligned}$$

$$EVSOC^t \geq 0 \ \forall \ t \in T \tag{33}$$
$$EVSOC^t \leq EVSOC_{max} + (100 - EVSOC_{max}) y^t_{EV\,float} \ \forall \ t \in T \tag{34}$$

$$\begin{aligned} EVSOC^1 = EVSOC\_last\_day: \ t^1_{start} > t^1_{end} \\ EVSOC^{t^1_{start}} = EVSOC_{ret}: \ t^1_{start} < t^1_{end} \end{aligned} \tag{35}$$

$$\begin{aligned} EVSOC^{t^s_{start}} = EVSOC^{t^s_{end}} - 100\frac{Km^s_{next} - Km^s_{fuel}}{Km^{100}} \ \forall \ s \in \{1, 2, \ldots, n_{trips}\} : t^1_{start} > t^1_{end} \\ EVSOC^{t^{s+1}_{start}} = EVSOC^{t^s_{end}} - 100\frac{Km^s_{next} - Km^s_{fuel}}{Km^{100}} \ \forall \ s \in \{1, 2, \ldots, n_{trips} - 1\} : t^1_{start} < t^1_{end} \end{aligned} \tag{36}$$

$$\begin{aligned} EVSOC^{t^s_{end}} \geq EVSOC^{end}_{min} \ \forall \ s \in \{1, 2, \ldots, n_{trips}\} \\ EVSOC^{t^{n_{trips}+1}_{end}} \geq EVSOC^{end}_{min} : t^1_{start} > t^1_{end} \end{aligned} \tag{37}$$

$$\begin{aligned} P^{ch,t}_{EVbat} \leq \frac{EVP^{ch}_{max}}{\eta^{ch}_{Ev}\mu_{Ev}} y^{ch,t}_{EVbat} \ \forall \ t \in T \\ P^{ch,t}_{EVbat} \geq \frac{EVP^{ch}_{min}}{\eta^{ch}_{Ev}\mu_{Ev}} y^{ch,t}_{EVbat} \ \forall \ t \in T \\ P^{dch,t}_{EVbat} \leq EVP^{dch}_{max} \eta^{dch}_{Ev} \mu_{Ev} y^{dch,t}_{EVbat} \ \forall \ t \in T \\ P^{dch,t}_{EVbat} \geq EVP^{dch}_{min} \eta^{dch}_{Ev} \mu_{Ev} y^{dch,t}_{EVbat} \ \forall \ t \in T \end{aligned} \tag{38}$$

$$y^{dch,t}_{EVbat} + y^{ch,t}_{EVbat} \leq 1 \ \forall \ t \in T \tag{39}$$

$$\begin{aligned} \varrho^t = 0 \ \forall \ s \in \{1, 2, \ldots, n_{trips}\}, t \in \{t^s_{end}, t^s_{end} + 1, \ldots, t^s_{start} - 1\}: \ t^1_{start} > t^1_{end} \\ EVSOC^t = 0 \ \forall \ s \in \{1, 2, \ldots, n_{trips}\}, t \in \{t^s_{end} + 1, t^s_{end} + 2, \ldots, t^s_{start} - 1\}: \ t^1_{start} > t^1_{end} \\ \varrho^t = 0 \ \forall \ t \in \left\{t^{n_{trips}+1}_{end}, t^{n_{trips}+1}_{end} + 1, \ldots, |T|\right\} : t^1_{start} > t^1_{end} \\ EVSOC^t = 0 \ \forall \ t \in \left\{t^{n_{trips}+1}_{end} + 1, t^{n_{trips}+1}_{end} + 2, \ldots, |T|\right\} : t^1_{start} > t^1_{end} \\ \varrho^t, EVSOC^t = 0 \ \forall \ t \in \left\{1, 2, \ldots, t^1_{start} - 1\right\} : t^1_{start} < t^1_{end} \\ \varrho^t = 0 \ \forall \ s \in \{1, 2, \ldots, n_{trips} - 1\}, t \in \{t^s_{end}, t^s_{end} + 1, \ldots, t^{s+1}_{start} - 1\} : t^1_{start} < t^1_{end} \\ EVSOC^t = 0 \ \forall \ s \in \{1, 2, \ldots, n_{trips} - 1\}, t \in \left\{t^s_{end} + 1, t^s_{end} + 2, \ldots, t^{s+1}_{start} - 1\right\} : t^1_{start} < t^1_{end} \\ \varrho^t = 0 \ \forall \ t \in \left\{t^{n_{trips}}_{end}, t^{n_{trips}}_{end} + 1, \ldots, |T|\right\} : t^1_{start} < t^1_{end} \\ EVSOC^t = 0 \ \forall \ t \in \left\{t^{n_{trips}}_{end} + 1, t^{n_{trips}}_{end} + 2, \ldots, |T|\right\} : t^1_{start} < t^1_{end} \end{aligned} \tag{40}$$

$$C^s_{ev} \geq Km^s_{fuel} P_{gas} \ \forall \ s \in \{1, 2, \ldots, n_{trips}\} \tag{41}$$

$$C_{ev} \geq \sum_{s=1}^{n_{trips}} C^s_{ev} \tag{42}$$

$$\begin{aligned} y^{dch,t}_{EVbat} \in \{0, 1\} \ \forall \ t \in T \\ y^{ch,t}_{EVbat} \in \{0, 1\} \ \forall \ t \in T \\ y^t_{EV\,float} \in \{0, 1\} \ \forall \ t \in T \\ C^s_{ev} \geq 0 \ \forall \ s \in \{1, 2, \ldots, n_{trips}\} \\ Km^s_{fuel} \geq 0 \ \forall \ s \in \{1, 2, \ldots, n_{trips}\} \\ C_{ev} \geq 0 \end{aligned} \tag{43}$$

Constraints (32) establish the relationships between the SOC, the discharging and charging powers, and the float loss. The vehicle could arrive without energy, so Constraints (33) place a lower bound of zero on the SOC. Constraints (34) place an upper bound on the float losses that is activated when a threshold is reached. Constraints (35) establish an initial value for the SOC. The former is activated when the first event is a departure, and the latter is activated when the first event is an arrival. Constraints (36) create a link between consecutive trips to ensure energy conservation. Constraints (37) place a lower bound on the SOC (sufficient to reach the nearest gas station) in intervals when travel is necessary. Constraints (38) establish bounds on the discharging and charging power. Constraints (39) ensure that at each $t \in T$ the battery either charges or discharges. Constraints (40) ensure null values for the intervals when the EV battery cannot be used. Constraints (41) calculate the fuel cost for each trip s. Constraint (42) gives the total cost of the fuel consumption. Constraints (43) are the binary and nonnegative restrictions.

An EV model is essentially the same as a battery model [9], but there are more constraints, including minimal SOC constraints and trip-signal constraints to ensure that the EV charges and discharges only when at home. Sousa et al. [80] present an EV model that is similar to a battery model. Our model is based on [9] and [80] and considers multiple trips in a day [59]. In addition, we consider hybrid vehicles.

2.9 Combined heat and power (CHP) Model

In this subsection, the CHP model is outlined. We explain also considerations and strategies used in the formulation. The CHP model is modeled by

$$\begin{aligned}
y^{\tau}_{CHP} \geq z^{t}_{CHP} \ \forall\ t \in T, \tau \in \{t, t+1, \ldots, \min\{t + \lceil d^{on}_{CHP}/\Delta t\rceil - 1, |T|\}\} \\
y^{\tau}_{CHP} \leq 1 - zd^{t}_{CHP} \ \forall\ t \in T, \tau \in \left\{t, t+1, \ldots, \min\left\{t + \left\lceil d^{off}_{CHP}/\Delta t\right\rceil - 1, |T|\right\}\right\} \\
z^{t+1}_{CHP} \leq 1 - y^{t}_{CHP} \ \forall\ t \in T\backslash\{|T|\} \\
zd^{t+1}_{CHP} \leq y^{t}_{CHP} \ \forall\ t \in T\backslash\{|T|\} \\
z^{t}_{CHP} \geq y^{t}_{CHP} - y^{t-1}_{CHP} \ \forall\ t \in T\backslash\{1\} \\
zd^{t}_{CHP} \geq -y^{t}_{CHP} + y^{t-1}_{CHP} \ \forall\ t \in T\backslash\{1\} \\
1 \geq zd^{t}_{CHP} + z^{t}_{CHP} \ \forall\ t \in T \\
z^{1}_{CHP} \geq y^{1}_{CHP} - y^{last_day}_{CHP}
\end{aligned} \tag{44}$$

$$\begin{aligned}
y^{1}_{CHP} = y^{ini}_{CHP} \\
P^{1}_{CHPe} = P^{ini}_{CHPe}
\end{aligned} \tag{45}$$

$$\begin{aligned}
P^{t+1}_{CHPe} \geq -\max\left\{P^{1,\mu}_{CHP,max}, P^{1,\eta}_{CHP,max}\right\} zd^{t+1}_{CHP} + P^{t}_{CHPe} - 60\Delta t_2 r^{down}_{CHP} w^{t}_{down} \ \forall\ t \in T\backslash\{|T|\} \\
P^{t+1}_{CHPe} \leq \max\left\{P^{1,\mu}_{CHP,max}, P^{1,\eta}_{CHP,max}\right\} z^{t+1}_{CHP} + P^{t}_{CHPe} + 60\Delta t_2 r^{up}_{CHP} w^{t}_{up} \ \forall\ t \in T\backslash\{|T|\} \\
1 \geq w^{t}_{up} + z^{t+1}_{CHP} \ \forall\ t \in T\backslash\{|T|\} \\
1 \geq w^{t}_{down} + zd^{t+1}_{CHP} \ \forall\ t \in T\backslash\{|T|\} \\
w^{t}_{up} \leq y^{t}_{CHP} \ \forall\ t \in T \\
w^{t}_{down} \leq y^{t}_{CHP} \ \forall\ t \in T
\end{aligned} \tag{46}$$

$$\begin{aligned}
P^{t}_{CHPe} \geq \max\left\{P^{1,\mu}_{CHP,max}, P^{1,\eta}_{CHP,max}\right\} y^{t}_{CHP} \ \forall\ t \in T \\
P^{t}_{CHPe} \leq \min\left\{P^{nb^{\mu}_{CHP},\mu}_{CHP,max}, P^{nb^{\eta}_{CHP},\eta}_{CHP,max}\right\} y^{t}_{CHP} \ \forall\ t \in T
\end{aligned} \tag{47}$$

$$\begin{aligned}
P^{t}_{CHPe} + P^{t}_{CHPt} = P^{t}_{CHP,fuel}\bar{\eta} \ \forall\ t \in T \\
P^{t}_{CHPt} = P^{t}_{CHPe}\bar{\mu} \ \forall\ t \in T
\end{aligned} \tag{48}$$

$$C^{t}_{CHP} \geq P^{t}_{CHP,fuel} P_{KW} \Delta t_2 \ \forall\ t \in T \tag{49}$$

$$\begin{aligned}
z^{t}_{CHP}, zd^{t}_{CHP} \in \{0,1\} \ \forall\ t \in T \\
y^{t}_{CHP} \in \{0,1\} \ \forall\ t \in T \\
w^{t}_{up}, w^{t}_{down} \leq 1 \ \forall\ t \in T \\
w^{t}_{up}, w^{t}_{down} \geq 0 \ \forall\ t \in T
\end{aligned} \tag{50}$$

Constraints (44) control the on/off status of the CHP. Constraints (45) initialize the status variable and the associated electricity production. Constraints (46) enforce ramp-up and ramp-down limits. Constraints (47) place bounds on the electricity generated by the CHP. Constraints (48) relate to the CHP operation. Constraints (49) measure the CHP fuel cost. Constraints (50) impose the variable domains.

Our model is based on [39] and [40] where efficiency is a function of the electrical power generated. The image of that function has values that are close to each other, so we consider the average efficiency to be a parameter rather than a variable. Variables z^{t}_{CHP} and zd^{t}_{CHP} can be relaxed because of Constraints (47).

2.10 Model for A_{IEUI}: Set of inelastic appliances with uninterruptible operation

The model for inelastic appliances with uninterruptible operation is outlined in this subsection.
With $\Phi_a = |T| - (\lceil D_a/\Delta t_2\rceil - 1)$, A_{IEUI} is modeled by

$$x^{t+h}_{a} \geq P^{h}_{a} y^{t}_{a} \ \forall\ a \in A^{t}_{IEUI},\ \forall\ t \in T,\ \forall\ h \in \{0, 1, \ldots, \lceil D_a/\Delta t_2\rceil - 1\} :\ t + h \leq |T| \tag{51}$$

$$x^{t}_{a} \leq \sum_{i=\max\{1, t-(\lceil D_a/\Delta t_2\rceil - 1)+1\}}^{t} P^{t-i}_{a} y^{i}_{a} \ \forall\ a \in A^{t}_{IEUI},\ \forall\ t \in T \tag{52}$$

$$y^{t}_{a} = 0 \ \forall\ a \in A^{t}_{IEUI}, t \in T : t > \Phi_a \tag{53}$$

$$\sum_{t=1}^{\Phi_a} y^{t}_{a} + \zeta_a = 1 \ \forall\ a \in A^{t}_{IEUI} \tag{54}$$

$$\sum_{tt=1}^{\Phi_a} tty_a^{tt} \geq \sum_{t=1}^{\Phi_b} ty_b^t + \lceil D_b/\Delta t_2 \rceil (1-\zeta_b) - |T| y_{b,a}$$
$$\forall\ a \in A^t_{IEUI},\ \forall\ b \in A^t_{IEUI},\ \forall\ k \in A_{IEUI} : a \in A^{t,k}_{IEUI}, b \in A^{t,k}_{IEUI} \quad (55)$$

$$\sum_{tt=1}^{\Phi_b} tty_b^{tt} \geq \sum_{t=1}^{\Phi_a} ty_a^t + \lceil D_a/\Delta t_2 \rceil (1-\zeta_a) - |T|(1-y_{b,a})$$
$$\forall\ a \in A^t_{IEUI},\ \forall\ b \in A^t_{IEUI},\ \forall\ k \in A_{IEUI} : a \in A^{t,k}_{IEUI}, b \in A^{t,k}_{IEUI} \quad (56)$$

$$\begin{aligned} U_a^t &\geq 0\ \forall\ a \in A^t_{IEUI},\ \forall\ t \in T \\ U_a^t &\geq S_a y_a^t - t y_a^t\ \forall\ a \in A^t_{IEUI},\ \forall\ t \in T \\ U_a^t &\geq -DS_a y_a^t + t y_a^t\ \forall\ a \in A^t_{IEUI},\ \forall\ t \in T \end{aligned} \quad (57)$$

$$\begin{aligned} \zeta_a &\geq 0\ \forall\ a \in A^t_{IEUI} \\ y_a^t &\in \{0,1\}\ \forall\ a \in A^t_{IEUI},\ \forall\ t \in T \\ y_{b,a} &\in \{0,1\}\ \forall\ a \in A^t_{IEUI},\ \forall\ b \in A^t_{IEUI}\ \forall\ k \in A_{IEUI} : a \in A^{t,k}_{IEUI}, b \in A^{t,k}_{IEUI} \end{aligned} \quad (58)$$

Constraints (51) and (52) assign the load profile of task $a \in A^t_{IEUI}$ to time $t \in T$. Constraints (53) eliminate solutions where the appliance cannot start its operation. Constraints (54) ensure that the task is done at most once, between the beginning of the horizon and the last start time permitting the completion of the task. Constraints (55) and (56) prevent overlap between tasks for the same appliance. Constraints (57) measure the discomfort arising from the deviation from the preferred time. Constraints (58) impose the variable domains.

A_{IEUI} is a set of inelastic appliances with uninterruptible operation (see [71]). In practice, the operation of these appliances is represented by a load profile. Load profiles forecast the power variation over a period of time for an appliance, frequently as an average. For example, Tsagarakis et al. [84] use aggregated load profiles, while [66] uses load profiles for specific machines. The former use a time-use survey (TUS) to construct the load profiles. However, the consumption found through TUS diaries can be distinct from the load measurements obtained by submetering [81]. The latter approach uses controlled tests to measure consumption, and the resulting profiles provide a good approximation. UK-DALE [45] is an open-access data-set giving the consumption of domestic appliances in the UK. The data are based on measurements of real electricity consumption.

Our model is task-oriented, an idea from [42] that proposes a model with parameters to indicate how many times each appliance will be used. In our case, we consider individual load profiles for each use of each appliance. Therefore, our model includes appliances that are used intermittently according to the classification in [71].

2.11 Model for A_{phases}: Set of appliances with interruptible phases operation

The model for appliances with interruptible phases operation is outlined in this subsection.
With $\mho_a^1 = |T| - \left(\left\lceil \sum_{p=1}^{PH_a} D_{a,p}/\Delta t_2 \right\rceil - 1\right)$, $\mho_a^2 = |T| - (\lceil D_{a,PH_a}/\Delta t_2 \rceil - 1)$, and $\mho_a^3 = (\lceil D_{a,PH_a}/\Delta t_2 \rceil)$, A_{phases} is modeled by

$$x_a^{t+h} \geq P_{a,p}^h y_{a,p}^t\ \forall\ a \in A^t_{Phases},\ \forall\ t \in T,\ \forall\ p \in \{1,2,\ldots,PH_a\},$$
$$\forall\ h \in \{0,1,\ldots,\lceil D_{a,p}/\Delta t_2 \rceil - 1\} :\ t+h \leq |T| \quad (59)$$

$$x_a^t \leq \sum_{p=1}^{PH_a} \sum_{i=\max\{1,t-(\lceil D_{a,p}/\Delta t_2 \rceil - 1)+1\}}^{t} P_{a,p}^{t-i} y_{a,p}^i\ \forall\ a \in A^t_{Phases},\ \forall\ t \in T \quad (60)$$

$$y_{a,p}^t = 0 \quad \forall\ a \in A^t_{Phases},\ \forall\ p \in \{1,2,\ldots,PH_a\},\ \forall\ t \in T : t > |T| - \left(\left\lceil D_{a,|PH_a|}/\Delta t_2 \right\rceil - 1\right) \quad (61)$$

$$\sum_{t=1}^{|T|-(\lceil D_{a,p}/\Delta t_2 \rceil - 1)} y_{a,p}^t + \Psi_{a,p} = 1\ \forall\ a \in A^t_{Phases},\ \forall\ p \in \{1,2,\ldots,PH_a\} \quad (62)$$

$$\sum_{tt=t}^{|T|} y_{a,p}^{tt} + \sum_{tt=1}^{t-1+\lceil D_{a,p}/\Delta t_2 \rceil} y_{a,p+1}^{tt} \leq 1\ \forall\ a \in A^t_{Phases},$$
$$\forall\ p \in \{1,2,\ldots,PH_a - 1\},\ \forall\ t \in T\ :\ t\ <\ |T| + 1 - \lceil D_{a,p}/\Delta t_2 \rceil \quad (63)$$

$$\sum_{tt=1}^{\mho_a^1} tty_{a,1}^{tt} \geq \sum_{t=1}^{\mho_b^2} ty_{b,PH_b}^t + \mho_b^3(1-\Psi_{b,1}) - |T|y_{b,a}^p$$
$$\forall\ a \in A_{Phases}^t,\ \forall\ b \in A_{Phases}^t,\ \forall\ k \in A_{Phases} : a \in A_{Phases}^{t,k}, b \in A_{Phases}^{t,k} \quad (64)$$

$$\sum_{tt=1}^{\mho_b^1} tty_{b,1}^{tt} \geq \sum_{t=1}^{\mho_a^2} ty_{a,PH_a}^t + \mho_a^3(1-\Psi_{a,1}) - |T|(1-y_{b,a}^p)$$
$$\forall\ a \in A_{Phases}^t,\ \forall\ b \in A_{Phases}^t,\ \forall\ k \in A_{Phases} : a \in A_{Phases}^{t,k}, b \in A_{Phases}^{t,k} \quad (65)$$

$$\begin{aligned} U_a^t &\geq 0\ \forall\ a \in A_{Phases}^t,\ \forall\ t \in T \\ U_a^t &\geq S_a y_{a,1}^t - t y_{a,1}^t\ \forall\ a \in A_{Phases}^t,\ \forall\ t \in T \\ U_a^t &\geq -DS_a y_{a,1}^t + t y_{a,1}^t\ \forall\ a \in A_{Phases}^t,\ \forall\ t \in T \\ U_a^t &\geq F_a y_{a,PH_a}^t - t y_{a,PH_a}^t\ \forall\ a \in A_{Phases}^t,\ \forall\ t \in T \\ U_a^t &\geq -DF_a y_{a,PH_a}^t + t y_{a,PH_a}^t\ \forall\ a \in A_{Phases}^t, t \in T \end{aligned} \quad (66)$$

$$\begin{aligned} \Psi_{a,p} &\geq 0\ \forall\ a \in A_{Phases}^t,\ \forall\ p \in \{1,2,\ldots,PH_a\} \\ y_{a,p}^t &\in \{0,1\}\ \forall\ a \in A_{Phases}^t,\ \forall\ t \in T,\ \forall\ p \in \{1,2,\ldots,PH_a\} \\ y_{b,a}^p &\in \{0,1\}\ \forall\ a \in A_{Phases}^t,\ \forall\ b \in A_{Phases}^t\ \forall\ k \in A_{Phases} : a \in A_{Phases}^{t,k}, b \in A_{Phases}^{t,k} \end{aligned} \quad (67)$$

Constraints (59) and (60) assign the load profile of each phase p of task $a \in A_{phases}^t$ to time $t \in T$. Constraints (61) eliminate solutions where the appliance cannot start its operation. Constraints (62) ensure that the task is done at most once, between the beginning of the horizon and the last start time permitting the completion of the task. Constraints (63), from [21], are precedence constraints between consecutive phases of the same task. Constraints (64) and (65) prevent overlap between tasks for the same appliance. Constraints (66) measure the discomfort arising from the deviation from the preferred time. Constraints (67) impose the variable domains.

Each load profile is separated into sequential phases, and the operation can be interrupted between phases. The appliances in A_{phases} include dishwashers [11], washing machines [69], and dryers [66].

2.12 Other constraints and objective function

Other constriants as well the objective function that are part of the whole optimization model are outlined in this subsection.

IBR constraints:

$$E_g^{t,i} \leq E_{th}^t\ \forall\ t \in T,\ \forall\ i \in B \quad (68)$$
$$\Delta t \sum_{t \in T} E_g^{t,i} \leq E\_bl^i\ \forall\ i \in B \quad (69)$$
$$\Delta t E_g^{t,i} \leq E\_bl^i y_g^i\ \forall\ t \in T,\ \forall\ i \in B \quad (70)$$
$$\sum_{i \in B} y_g^i \leq 1 \quad (71)$$
$$y_g^i \in \{0,1\}\ \forall\ i \in B \quad (72)$$

Constraint (68) limits the energy that can be bought. Constraints (69) to (72) are the main IBR constraints: (69) ensures that the daily consumption is within the capacity; (70) controls the activation of the blocks; (71) ensures that at most one block is used; and (72) are the binary restrictions.

Flow Conservation:

$$\sum_{a \in A} x_a^t = 10^3(p_{EVbatt}^{ch,t} + P_{bat}^{ch,t} - P_{bat}^{dch,t} - p_{EVbatt}^{dch,t} - P_{CHPe}^t) + E_{pv}^t - E_v^t + E_{wt}^t + \sum_{i \in B} E_g^{t,i}\ \forall\ t \in T \quad (73)$$

The coupling constraints (73) ensure energy conservation.

Financial Incentives:

$$C^t = \Delta t \left[\lambda^t \left(\sum_{i \in B} (1-\varpi^i) E_g^{t,i} \right) - \nu^t E_v^t \right] \forall\ t \in T \quad (74)$$
$$E_v^t \leq E_{th}^t\ \forall\ t \in T \quad (75)$$

Constraints (74) represent the cost at each time t, given by the energy acquisition cost for block i minus the energy sold plus the price of CHP. Constraint (75) limits the energy that can be sold. Variable E_v^t represents

the case where the customer can inject electricity into the grid. In some markets, the customer receives in exchange an energy credit for future consumption. In this case, we set $E_v^t = 0$, add $E_{av}^{t-1} - E_{av}^t$ in the right hand side of (73) and replace Constraint (75) by $E_{av}^0 = 0$ to initialize the power credit variable.
Objective function:

$$\min_{\Xi} w_c \left(\sum_{t \in T} C^t + C_{ev} + C_{CHP}^t \right) + w_t \sum_{t \in T} \sum_{a \in A} V_a^t + w_u \left(\sum_{a \in A_{phases}^t} \sum_{p=1}^{|PH_a|} \Psi_{a,p} + \sum_{a \in A_{IEUI}^t} \zeta_a + \sum_{t \in T} \sum_{a \in A^t} U_a^t \right) \quad (76)$$

We minimize a weighted sum of comfort and cost (76), where the cost is given by (74) and the EV cost.

3 Data and Instances

In this section we discuss our data and how we create the instances.

3.1 Locations

Brazil will be one of the largest smart-grid markets by 2023 [35]. The country has a total installed capacity of 161 GW [7], which is expected to grow to 224 GW by 2030 [32, Table 6.26] via initiatives such as the Cities of the Future Project [17]. An analysis of the smart grid stage in Brazil appears in [28]. The climatic data was taken from [5, Chapter 14]. We calculated the temperature based on 5% dry-bulb design conditions. The wind speed data was taken from [50].

3.2 Prices

In Brazil, there are two pricing options: the conventional tariff and the white tariff. The conventional tariff is constant, whereas the white tariff is a TOU pricing with a single price for weekends and holidays and three weekday prices:

1. Peak hours: Three consecutive daily hours defined by the distributor.
2. Intermediate peak hours: The hour before and the hour after the peak hours.
3. Nonpeak hours: The remaining hours of the day.

We use the electricity prices published in April 2017 for the white tariff. We summed two tariffs, following [53, p. 57].

The IBR pricing defined by federal law [15] specifies certain discounts:

1. For the portion of consumption below 30 kWh/month, the discount is 65%.
2. For the portion between 31 and 100 kWh/month, the discount is 40%.
3. For the portion between 101 and 220 kWh/month, the discount is 10%.

We divided the monthly limits defined above by 30 days. This makes our model less realistic, but since smart meters track and report energy consumption in minutes, we assume that a pricing scheme over a day will be more important than one for the whole month. The law applies to a subgroup of the population, but we apply it to everyone.

Brazil has a net metering incentive. If the electricity bought from the grid is less than that injected, the customer receives an energy credit for future consumption. In addition, we assume that, as in other markets, Brazil's consumers will in the future have the opportunity to sell electricity, i.e., a *feed-in tariff*. Thus, we consider $\nu^t = \lambda^t/2$ for all $t \in T$.

3.3 Capacity

We set the capacity E_{th}^t to 75 kW, which is the residential capacity in Brazil.

3.4 PV and Solar Collector

We take the data from data-sheets or use the estimates in [30]. We consider the PVs *Canadian Solar CS5P250M*, *Yingli Solar JS150*, and *Siemens SM110* and the solar collectors *CSi Sodramar*, *TERMOMAX*, *Soletrol*, and *Sunda Seido 10*. The ground reflectance was generated from the uniform distribution U(0.13,3) according to [5, Table 5, Chapter 14].

3.5 Wind Turbines

The data comes from the data-sheets for the *Raum Energy 3.5 kW Wind Turbine System* and the *Raum Energy 1.3 kW Wind Turbine System*.

3.6 HVAC

For the house, we generated resistance values from a uniform distribution (see [75]), converting the units to (m^2 ^{o}C.h/J). The house height is 3.048 m, with $A_{ceiling} = A_{floor} = 100$ m^2. We set $P_{heating} = P_{cool} = 60\,W/m^2 \times A_{floor}$, an approximate value suggested by some manufacturers. We set A_{ul} between 0.7 and 2.8. We set IDF to 0.031 for cooling and 0.086 for heating. The other parameters are $T_f^t = 23^oC\ \forall\ t \in T$, $H_p^t = 97.57\,W\ \forall\ t \in T$.

3.7 Water Heaters and Shower

We use $T_f^{chu} = T_f^{wh} = 50^oC$ (see [51]). We set $P_{wh} \sim U(4000, 5000)\,W$ (see [75]). The heat resistance is given by $U(12, 25)^oFft^2h/Btu$ converted to (m^2 ^{o}C.h/J). We take the WH area and diameter from the data-sheets for Giant-142ETE, Giant-152ETE, Giant-172ETE, Rheem-PROPH50, Rheem-PROPH65, and Rheem-PROPH80. We use the diameter to calculate $(UA)_{wh}$ and V_{tank}. We set $T^{max} = 100^oC$ and $E_{wh} = 1$.

We took the temperature of the water from the street (T_{inlet}^t) from [23, Graphic 4]. We projected the missing intervals so that the last projected value is equal to the first collected value.

For fr_{wh}^t and fr_{chu}^t, we used the data available in [27]. For each client, we aggregate the daily consumption in intervals of Δt. Inter-period consumption is calculated proportionally. P_{chu} is obtained from the data-sheets for Lorenzetti's showers.

3.8 Batteries

We used the following values from [93]: $E_{bat} = 24$ kWh, $SOC_{min} = 20\%$, $SOC_{max} = 100\%$, $p_{max}^{ch} = 4$ kW, $p_{max}^{dch} = 4$ kW, $p_{min}^{ch} = 0.3$ kW, $p_{min}^{dch} = 0.3$ kW, $\eta^{ch} = 0.91$, $\eta^{dch} = 0.91$, $\mu = 1$. According to [16], in a low-storage system the float charge losses represent around 100 W, so $p_{loss} = 0.1$ kW.

3.9 Fridge

The fridge is described in [14] and [13]. The other parameters are $T_{freezer}^{start} = -13^o$C, $T_{refri}^{start} = 6^o$C, $P_{comp} \sim U(150, 170)$ W considering the permanent regime from [22], $T_f^{freezer} = -18^o$C, and $T_f^{refri} = 2^o$C.

3.10 Electric Vehicles

We used the Nissan Leaf's battery specifications [62]: $EV_{bat} = 24$ kWh, $EVSOC_{max} = 90\%$, $EVSOC_{min} = 0\%$ and $EVP_{max}^{ch} = EVP_{max}^{dch} = 3.6$ kW. The other parameters are based on the battery parameters: $EVP_{min}^{ch} = EVP_{min}^{dch} = 0.3$ kW, $EV\mu = 1$, and $EVp_{loss} = 0.1$ kW.

The range of the Leaf model is 160 km and its battery capacity is 24 kWh [80]. We calculated $km^{100} = EV_{bat}/Electricity\ consumption = (24\,kWh)/(150\,Whkm^{-1}) = 160$ km, as in [80].

We simulated the battery-charging model for 7 h. At time 0, the SOC was 0. With the specified rate of 3.6 kW/h, the SOC should be 25.2 kWh after 7 h. We therefore defined $\eta_{ev}^{dch} = 24/25.2 \approx 0.95$. Moreover, we set $\eta_{ev}^{dch} = \eta_{ev}^{ch}$.

The number of trips is set to $n_{trip} \sim U(1, 4)$ and t_{start}^s and t_{end}^s are generated randomly. The first trip has a minimum duration of 8 h, the second 4 h, the third 1 h, and the fourth 0.5 h.

The other parameters are $price\_gas = 3$ \$/l, $cons\_gas = 10$ km/l, $EVSOC\_last\_day = 50\%$, $Km_{next}^s \sim U(0, km^{100})\,km\ \forall\ s \in \{1, ..., n_{trip}\}$, $EVSOC_{min}^{end} \sim U(EVSOC_{ret}$,MM)%, where MM = maximum value of $EVSOC_{ret}$, and finally, $EVSOC_{ret} \sim U(0, 30)\%$.

3.11 CHP

We take the data from [40, Table 4] and the data-sheet for CHP CP5WN-SPB. For that CHP, $rate_{CHP}^{fuel} = \frac{0.72\,gallon/h}{17.8\,kWh} = \frac{3.79\,l/gallon \times 0.72\,gallon/h}{17.8\,KWh} = 0.153\,l/kWh$.

Thus, the values are: $d_{CHP}^{on} = d_{CHP}^{off} = 60$ min, $nb_{CHP}^{\mu} = nb_{CHP}^{\eta} = 3$, $r_{CHP}^{down} = r_{CHP}^{up} = 0.05$ kW/min, $y_{CHP}^{last\_day} = y_{CHP}^{ini} = 0$, and $P_{CHPe}^{ini} = 0$ kW. Fixing μ and $\eta \in \{1, 2, 3\}$ we set $P_{CHP,min}^{k,\mu}$ and $P_{CHP,min}^{k,\eta} \in \{0, 0.2, 0.5\}$ kW, $P_{CHP,max}^{k,\mu}$ and $P_{CHP,max}^{k,\eta} \in \{0.2, 0.5, 1\}$ kW, $\eta_{CHP,p}^k \in \{0, 80, 85\}$, and $\mu_{CHP,p}^k \in \{0, 40, 35\}$.

We set the overall efficiency to the average of the efficiencies given by the piecewise linear function, discarding null efficiencies. Thus, $\bar{\eta} = 0.825$ and $\bar{\mu} = 0.375$.

3.12 A_{IEUI} and A_{phases}

We use the data from [45]. We start the analysis from the first day that has measured data at midnight. Missing data is assumed to indicate no consumption. We aggregated the power data into 10-min intervals based on the average values. We calculated probabilities for the time and duration of the use of each appliance. Using these probabilities, we chose values for S_a, the preferred starting time, and D_a, the duration of use. We obtain P_a^h from the aggregated power in the interval between t and $t + D_a$. Finally, we set $DS_a = D_a + U(0, 4)$.

For A_{phases}, we performed the steps above for each phase. Dishwashers have three phases: washing, draining, and drying [11]. Washing machines have three phases: water heating, washing, and spinning [69]. Dryers have two phases: with and without heat [66]. In [66], the duration of the dryer's second phase is between 5 and 15 min, so we consider the final 10 min of the load profile to be the second phase.

4 Results and Discussion

The scheduling problem is solved in this section, using various models. We selected the references from Table 1 with at least seven submodels. For a fair comparison, we replaced the comfort constraints in every model by a fixed start time for the appliances based on load profiles, and fixed bounds for desired temperatures for the thermal appliances. Thus, comfort is equivalent for every model and the objective function considers only the cost. The parameters not previously defined are as follows: $H = 24$, $|T| = 2$, and $w_c = w_u = w_t = 1$. Each instance has the same set of features for each model compared: same parameters for prices, same set of appliances, etc.

4.1 Models from [76]

In this subsection, we compare results using our models and models from [76]. We consider the appliance models in [77, 76] with the following adjustments:

1. We assume that $S_t^{ESS} = S_t^{ess}$.
2. The available data corresponds to time windows and power for the four appliances in [76, Table 1] and electricity prices in [76, Figure 3]. Since the devices based on load profiles have a fixed usage initialization, we use the data from Section 3 instead of that from [76].
3. For the freezer and fridge, the computation of β^{fr}, α^{fr} and γ^{fr} is not specified. We assume that β^{fr} is related to the action of opening and closing the fridge doors, α^{fr} is related to the evaporator temperature, and γ^{fr} is related to the losses.
4. For HVAC, α^{ac} and α^{ht} are undefined. We assume that $EP_t = EP_t^{\Theta} : \Theta \in \{\text{ac, ht}\}$. The parameters β^{ac}, β^{ht}, ρ^{ac}, and ρ^{ht} are computed as in our model, considering infiltration and losses based on the structure of the house.
5. For lighting, there is no constraint that associates illumination level with consumption. Therefore, we do not consider this.

We start our experiments with an "initial" combination composed of A_{IEUI}, fridges, WTs, PVs, IBR constraints, and selling options. We progressively add more appliances. For example, in Table 2, Ins. 2 includes the appliances considered in Ins. 1 plus an ESS.

Table 2: Costs for model from [76] and our model.

Ins.	Combination	[76] cost ($)	Our cost ($)
1	"initial"	4.02	4.02
2	Ins. 1 + ESS	1.61	1.49
3	Ins. 2 + HVAC	1.93	6.83
4	Ins. 3 + CHP, WH	1.93	6.83
5	Ins. 4 + A_{phases}, Shower	-	9.06
6	Ins. 5 + EV	-	30.03
7	Ins. 4 + Boiler, TSS	1.93	-

In Ins. 1, we assign consumption profiles over the horizon and respect the bounds on the freezer and fridge temperatures. Both models give the same cost.

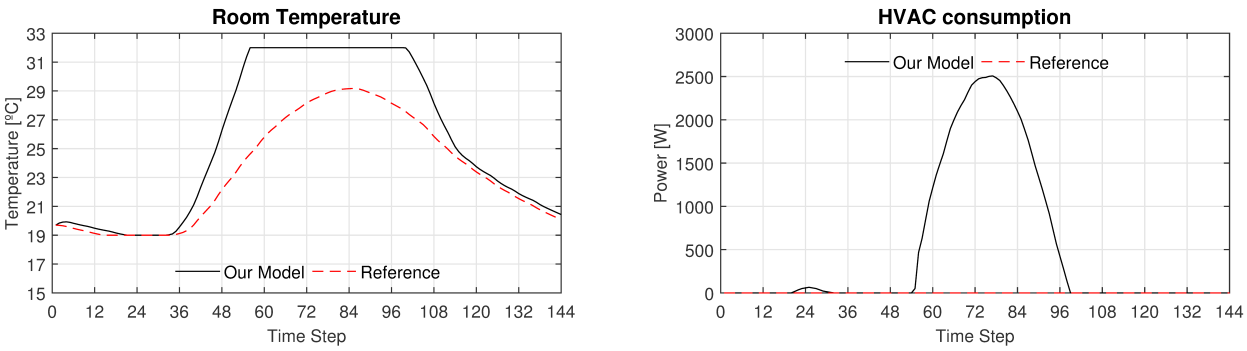

Figure 5: Results for temperature of Ins. 9.

In Ins. 2, we add a battery, a type of ESS. The efficiencies for the discharging and charging operations are set to 100%. The model of [76] allows the battery to be off during the entire horizon, but with charging and discharging. Their cost is 8% higher than ours. There are two reasons for this. First, our model considers the SOC at the beginning of an interval, whereas [76] considers it at the end. Thus, in the final interval our model records a discharge while the model from [76] does not. Second, we have lower bounds on the charge and discharge variables. If we remove these two differences, we find the same solution.

In Ins. 3, for the model of [76], HVAC adds 32 cents to the bill while our model adds around 440 cents. Like the ESS, the HVAC is off throughout the horizon, but it contributes to the indoor temperature. As we will see in Ins. 9, the main issue in this experiment is the solar gain.

In Ins. 4, both models adjust the use of fridge and batteries, achieving the same cost as in Ins. 3.

In Ins. 5, 6, and 7, we add appliances that are considered either by our model or by [76], obtaining results for just one of the models.

In Ins. 3, the HVAC and the battery cannot emit or absorb energy if they are not turned on. For example, a battery could have the constraint set $AC_b = \{\text{BatPower}_t \leq \text{BatCapacity} \times y_t^{\text{on,off}} \forall\ t \in T\}$, where $y_t^{\text{on,off}}$ is binary, and similar steps give the constraint set AC_h for HVAC. Table 3 shows the results when we add the sets AC_b and AC_h.

Table 3: Costs for model from [76] and our model, with additional constraints from [76].

Ins.	Combination	[76] cost ($)	Our cost ($)
1	"initial"	4.02	4.02
8	Ins. 1 + ESS, AC_b	2.13	1.49
9	Ins. 8 + HVAC	2.13	6.83
10	Ins. 9 + AC_h	infeasible	6.83
11	Ins. 8 + solar gain	infeasible	6.83
12	Ins. 10 + disjoint set	2.28	6.83
13	Ins. 12 + solar gain	7.34	6.83

For Ins. 8, we note that the model from [76] has a cost around 43% higher than ours. The cost for [76], compared with Ins. 2, is increased because of the battery losses. For Ins. 9, HVAC works without consumption because the activation constraints are not considered. When we add these constraints in Ins. 10, [76] becomes infeasible. Moreover, in Ins. 9, our model consumes energy trying to keep the indoor temperature within the bounds. This does not happen in [76], as shown in Figure 5. The model from [76] does not consider solar gain. This has a considerable effect on the indoor temperature [8], so our model consumes more energy and is more expensive.

When we add solar gain in Ins. 11, [76] becomes infeasible. Ins. 12 assumes that the time windows (TWs) for the A/C and heating form a disjoint set. The model from [76] now gives a feasible solution. However, there is still no consideration of solar gain, and finding the optimal disjoint set of TWs is difficult since there are $2^{|T|}$ possible combinations. If we remove the solar gain from the analysis, our model decreases the cost by around 280%. Ins. 13 adds solar gain to Ins. 12 with only A/C for the disjoint set of TWs for the HVAC to avoid infeasibility. The model from [76] becomes, monetarily, more expensive than ours.

The thermal energy storage model in [76] follows the ESS model, so a similar analysis can be performed. The CHP in [76] comes from [48], and we present this analysis in Section 4.3. Although the model from [76] gives a cost that is lower by about R$1715 (544USD), our model is more realistic.

4.2 Models from [8, 9]

In this subsection, we compare results using our models and models from [8, 9]. The models from [8, 9] consider equivalent batteries, WH, and underfloor HVAC models. Moreover, they have the same energy flow conservation constraints.

We discussed the limitations of the battery models in Section 2.6. The WH model from [8, 9] is $T_{st}(t+1) = T_{st}(t) + \frac{V_D^{th}(t)}{(V_{tot})}(T_{cw} - T_{st}(t)) + \frac{P_{aux}^{th}(t)+P_{CHP}^{th}(t)}{V_{tot}C_w} - \frac{A_{st}}{R_{st}}(T_{st}(t) - T_b(t)) \; \forall \; t \in T\backslash\{|T|\}$, where V_{tot} is the total WH volume; $V_D^{th}(t)$ is the hourly hot water demand at time t; $T_{cw}(t)$, $T_b(t)$, and $T_{st}(t)$ are the entering cold water, environment around the WH, and hot water temperatures at time t, respectively; A_{st} is the surface area of the WH; and R_{st} is the thermal resistance of the WH insulation material. Using our parameter Δt_2, we have:
$T_{st}(t+1) = \frac{V_D^{th}(t)}{(V_{tot})}(T_{cw} - T_{st}(t)) + \Delta t_2 \frac{P_{aux}^{th}(t)+P_{CHP}^{th}(t)}{V_{tot}C_w} - \frac{\Delta t_2}{V_{tot}C_w}\frac{A_{st}}{R_{st}}(T_{st}(t) - T_b(t)) + T_{st}(t) \; \forall \; t \in T\backslash\{|T|\}$. Note that multiplying demand by the time interval results in V_D^{th}. Also, we use an electrical resistance as the auxiliary power while [8, 9] use a boiler fed by gas. Since gas and electricity have different prices, for a fair comparison, we assume that the three WH models ([9], [8], and ours) use electricity as auxiliary power. Note that the three models link the HVAC and CHP systems.

Our HVAC is directly in contact with the air that heats the principal floor, while the HVACs from [8, 9] are on the basement floor. Otherwise, the models are equivalent. For a fair comparison, we assume that all the models have the HVAC on the main floor.

The CHP model in [9] differs from that in [8] by a binary on/off variable and one constraint. We test both versions. The *schedulable tasks and residential load* model has more constraints in [9] than in [8], but as we set the starting time for the appliances based on the load profiles, the models are feasible.

Finally, since [8] considers WTs and PVs, we add these to [9]. The conservation constraints for both come from [8, Equation 37] with $\delta = 1$.

We start our experiments with an "initial" combination composed of the A_{IEUI} and A_{phases} appliances, WTs, PVs, IBR constraints, and selling options. We progressively add more appliances; see Table 4.

Table 4: Costs for models from [8, 9] and our model.

Ins.	Combination	[9] cost ($)	[8] cost ($)	Our cost ($)
1	"initial"	3.9506	3.9506	3.9506
2	Ins. 1 + ESS	-5.2055	-5.2055	1.3134
3	Ins. 2 + SOC_{min}	1.3102	1.3102	1.3134
4	Ins. 3 + D_A	1.2716	1.2716	2.0013
5	Ins. 1 + HVAC	8.7767	8.7767	8.7767
6	Ins. 3 + HVAC	6.6601	6.6601	6.6629
7	Ins. 6 + D_A	6.5999	6.5999	7.3859
8	Ins. 5 + WH, $\text{CHP}_{\text{ini}}^{\text{off}}$	16.6304	infeasible	9.7961
9	Ins. 5 + WH, $\text{CHP}_{\text{ini}}^{\text{on}}$	infeasible	infeasible	10.5269
10	Ins. 9 + D_A	infeasible	infeasible	-4.4723
11	Ins. 8 + D_A	16.6304	infeasible	-2.4028

In Ins. 1, we assign consumption profiles over the horizon. All the models give the same cost.

In Ins. 2, we add a battery. The efficiencies for the charging and discharging operations are, again, set to 100%. For [8, 9] we do not place an upper bound on the initial SOC. Their SOC starts at the maximal value allowed, which gives a result 296% cheaper than our model.

Suppose SOC_{min} is the bound on the initial SOC. We add SOC_{min} to the models from [8, 9] in Ins. 3. Then, their results are 0.24% cheaper than our result because they do not specify a minimal power for the charging and discharging variables. If we also add these constraints, we obtain the same cost as for our model.

In Ins. 4, we change the efficiencies to the values in [9]. D_A refers to the data from [9]. Their cost is 36.5% lower than our cost. The most important part of this difference is explained by the energy construction in the battery constraints linked with the energy conservation flow in [8, 9] (see Section 2.6).

In Ins. 5 and 6, we test HVAC and HVAC with ESS, respectively. The efficiencies in the battery model are 100%. The results are identical for Ins. 5, and they are slightly different for Ins. 6 for the same reason as in Ins. 3. However, for Ins. 7, with D_A, the [8, 9] results are 10.6% cheaper than ours because of the energy creation.

In Ins. 8, we test the CHP with the WH and HVAC. The CHP is off in the first interval, indicated by $\text{CHP}_{\text{ini}}^{\text{off}}$ in Table 4. In the [9] results, CHP and the boiler were not used. The only way to increase the water temperature is by increasing the room temperature, but this solution is 69.8% more expensive than our solution. In [8] the ramp-up constraints do not allow the start-up of the CHP. Moreover, the off status is not allowed. Therefore, the [8] model is infeasible.

In Ins. 9, we changed the CHP status at the first interval. It is on with a maximal production of electrical power, indicated by $\text{CHP}_{\text{ini}}^{\text{on}}$ in Table 4. Constraint 17 from the [9] model makes the problem infeasible, and the upper bound on P_{CHPt}^{t} in the [8] model makes the problem infeasible.

Ins. 10 and 11 are identical to Ins. 8 and 9, but with D_A. The analysis for Ins. 8 and 9 applies. For Ins. 11, our model sells electricity while the [9] model buys it. Our solution is around 114% (R$19.03) less expensive than the [9] solution. This represents an annual cost of ≈ R$6947 (2205 USD).

4.3 Models from [48]

In this subsection, we compare results using our models and models from [48]. There are two models from [48] that we did not consider in the analysis: the fridge model (29–31 in [48]) and the HVAC model (32–33 in [48]). These models have a scheduled consumption solution as input. For each interval, the models postpone or advance the time when the appliance will be turned on in that input solution. Thus, [48] assumes that the cooling goods (food), for the fridge, and the living space (air), for the HVAC, have enough thermal inertia to act as a buffer. We do not know how to determine the initial buffers, needed as parameters. We assume we have a scheduled solution for the fridge and a null initial buffer for the cooling goods. We consider only a fridge, and we optimize the electricity cost using the models from [48] and our model. The solution found by [48], shown in Figure 6, is not feasible because the temperatures become too high.

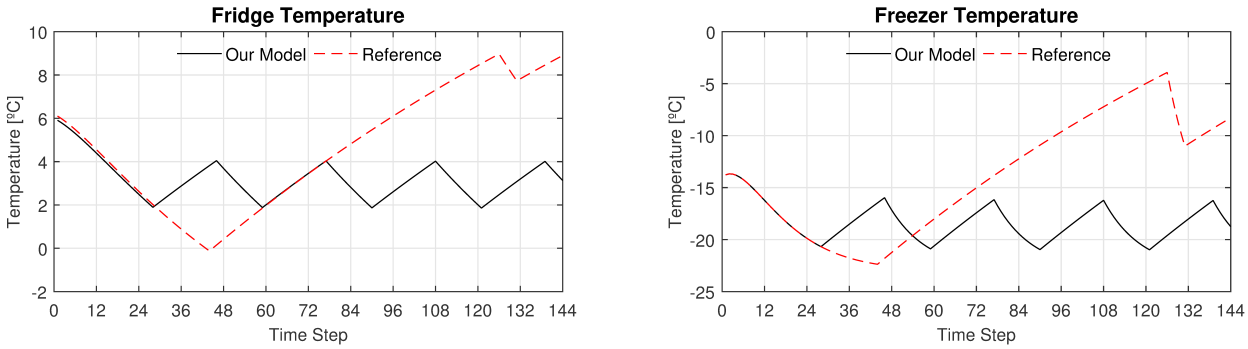

Figure 6: Results for temperature of reference fridge model from [48] and our model.

We started our experiments with an "initial" combination composed of the A_{IEUI} and PV appliances, IBR constraints, and selling options. WTs are considered in all the instances except 1, 2, 3, and 6. We progressively add more appliances; see Table 5.

In Ins. 1, we assign consumption profiles in the horizon and consider the production from the PV. Both models give the same cost.

In Ins. 2, we add the ESS. In contrast to [76], the ESS model in [48] is designed specifically for a flywheel. The [48] solution continuously charges and discharges simultaneously to maintain feasibility. It is 1.12 times more expensive than our solution.

Given the continuous charging and discharging operation of Ins. 2, in Ins. 3 we assume that the ESS power variables in [48] should be allowed to be zero, allowing the model to either charge or discharge. We change Constraints 10 from [48] to: $y_t p_{min}^{ess,r} \leq p_t^{ees,r} \leq y_t p_{max}^{ess,r} \; \forall \; r \in \{eex, eim\}, t \in T$, where $y_t \in \{0,1\}$ is an on/off variable at time t. This is represented by ESS* in Table 5. In [48], the battery does not always charge and discharge at the same time. This explains the cost decrease compared to Ins. 2.

Ins. 4 uses the appliances from Ins. 1 plus CHP. The CHP is off in the first interval. The costs for the two models are almost the same. In our model CHP is used between intervals 99 and 123, and in the [48] model CHP is not used. This will be discussed in our analysis of Ins. 11.

In Ins. 5, we add the production from WT. There is no WT in [48], but it decreased the cost by a factor of 4 compared with the cost for Ins. 1. We therefore considered WT for the next experiments.

In Ins. 6, we add ESS to Ins. 5. The [48] solution continuously charges and discharges at the same time to maintain feasibility: it is 5.6 times more expensive than our solution. The difference between the [48] solution and our solution is larger in Ins. 6 than in Ins. 2. Moreover, we can compare the cost reduction after the addition of WT, using the results from Ins. 2 and 6. We reduced the cost by a factor of 13 while the [48] model reduced it by 2.6. This is because when there is energy coming from WT, the battery has to be used more to sell energy at high prices. If the battery model has limitations, increased use of the battery will have an impact on the cost. If batteries are not considered, the differences are reduced, as shown by the solutions for Ins. 4 and 11.

We use ESS* for Ins. 7, as in Ins. 3. Compared to Ins. 6, the results do not change because $y_t = 1 \; \forall \; t \in T$. In Ins. 8, 9, and 10, the addition of EVs makes the models from [48] infeasible. We will explain this below.

Ins. 11 has the same appliances as Ins. 5 plus CHP. The CHP is off in the first interval. Our model and the [48] model give similar costs. In our model CHP is used between intervals 113 and 118; in the [48] model

Table 5: Costs for model from [48] and our model.

Ins.	Combination	[48] cost ($)	our cost ($)
1	"initial"	12.6557	12.6557
2	Ins. 1 + ESS	11.6846	10.4669
3	Ins. 2 + ESS*	11.6463	10.4669
4	Ins. 1 + CHP	12.6557	12.3806
5	Ins. 1 + WT	3.5393	3.5393
6	Ins. 5 + ESS	4.5219	0.8055
7	Ins. 6 + ESS*	4.5219	0.8055
8	Ins. 6 + EV	infeasible	21.8308
9	Ins. 8 + CHP	infeasible	21.8308
10	Every appliance	infeasible	30.0261
11	Ins. 5 + CHP	3.5393	3.521
12	Ins. 11 + off grid, WS	infeasible	20.7146
13	Ins. 5 + EV	infeasible	23.3725
14	Ins. 5 + EV	infeasible	3.9683
15	Ins. 5 + EV*	11.0408	3.9683
16	Ins. 15 + ESS	10.6995	2.7601
17	Ins. 16 + CHP	10.6995	2.7601

it is not used. This is because the ramp-up and ramp-down constraints in [48] do not allow the CHP to change state. This can be problematic when there is more demand or in off-grid systems.

In Ins. 12, we force the use of CHP via an off-grid system. If a surplus of energy occurs, it is lost, i.e., we waste the surplus (WS). Since fuel is more expensive than electricity in our data, the cost of meeting the demand is higher, and it cannot be met by the [48] model because of the ramp-up and ramp-down constraints.

In Ins. 13, we consider the appliances from Ins. 5 plus EV. The infeasibility in the [48] model is because that model cannot consider the case where the vehicle departs at time k_0, returns at time k_1, and departs again at time k_2 ($k_2 > k_1 > k_0$). This implies noncyclic behavior since there is an odd number of departure-arrival events. The bounds $E_t^{evh,ub}$ and $E_t^{evh,lb}$ in the [48] model cannot handle this case.

In Ins. 14, we change the EV parameters to allow only one departure, where the vehicle is plugged in at interval 7 and the departure is at interval 110. Here, the scenario is appropriate for the [48] model, but there is no zero energy assignment when the EV is traveling because of Constraint 22 from [48]. In Ins. 15, we changed this constraint to: $e_t^{evh} = e_{t-1}^{evh} + (p_t^{evh,eex}\eta^{evh,eex} - \frac{p_t^{evh,eim}}{\eta^{evh,eim}})\Delta t_2 + k_t^{evh}(E_t^{evh,ub} - e_{t-1}^{evh})\ \forall\, t \in T$. This change is indicated by EV* in Table 5. It corrects the problem of Ins. 14, but the inequalities 21 from [48] do not allow the power variables to be zero. This increases the cost, and our cost is around 278% cheaper.

Ins. 16 adds ESS to Ins. 15; Ins. 17 adds CHP to Ins. 16. For both models, ESS reduces the final cost, but CHP does not (it is not used). Our cost is 389% (R$7.93) cheaper. This represents an annual cost of $\approx$ R$2894 (918 USD).

4.4 Application: Day-to-day scheduling

We now present an application of our model to a house in Belo Horizonte, Brazil, during the summer. We used a computer equipped with an 1.9 Ghz Intel Core i5-4300U CPU. Figures 7 and 8 show the forecast data, the electricity price, and the behavior of the appliances in the optimal solution.

In the Water Temperature and Water Temperature in Shower plots, a Temp. wish value of zero means that the user does not care about the temperature. The plots show that the temperature needs are almost met. For instance, the water temperature is acceptable for the shower and for general use after step 36. The temperature before step 12 is unacceptable because the WH power and the thermal energy provided by CHP cannot sufficiently increase the initial temperature in the interval before the first and second uses. This is confirmed by the plot *Fraction of time with power on*, which shows that WH is on from the start until near step 12. The CHP operates at a maximal speed until step 12. The air temperature deviates from the target around 12 a.m. because the A/C power is insufficient. Note that in *Fraction of time with power on* the A/C is on whenever the temperature is above the target. The fridge and freezer quickly adjust their internal temperatures.

Discharge mode is preferred for the batteries when the price is high. The customer does not buy energy between steps 96 and 125 because it is too expensive. Moreover, CHP is preferred around those times. The EV makes its planned trips and is used for storage when electricity is expensive, e.g., in the steps around 100. The appliances with load profiles are used during the permitted time windows.

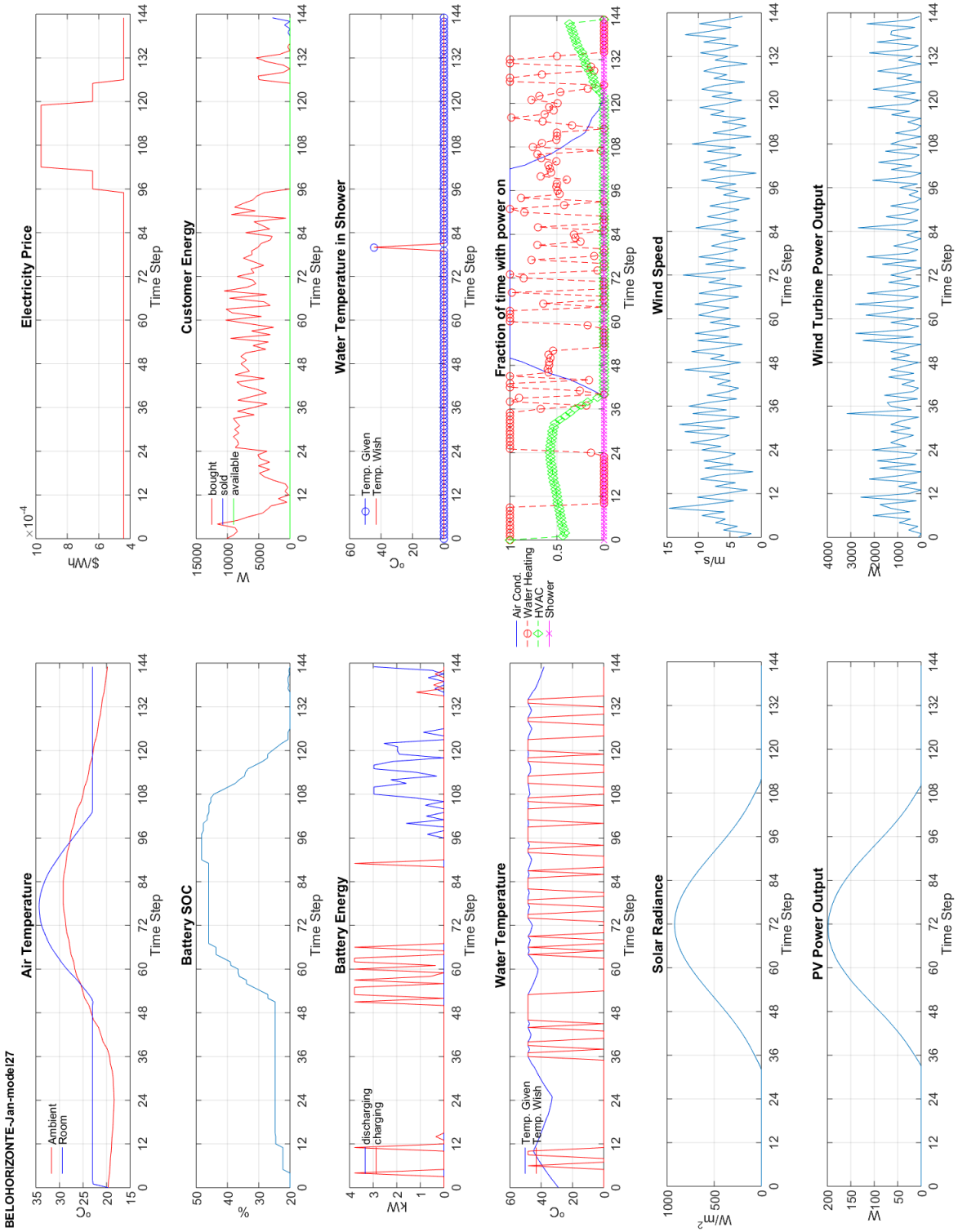

Figure 7: Results for Belo Horizonte in January.

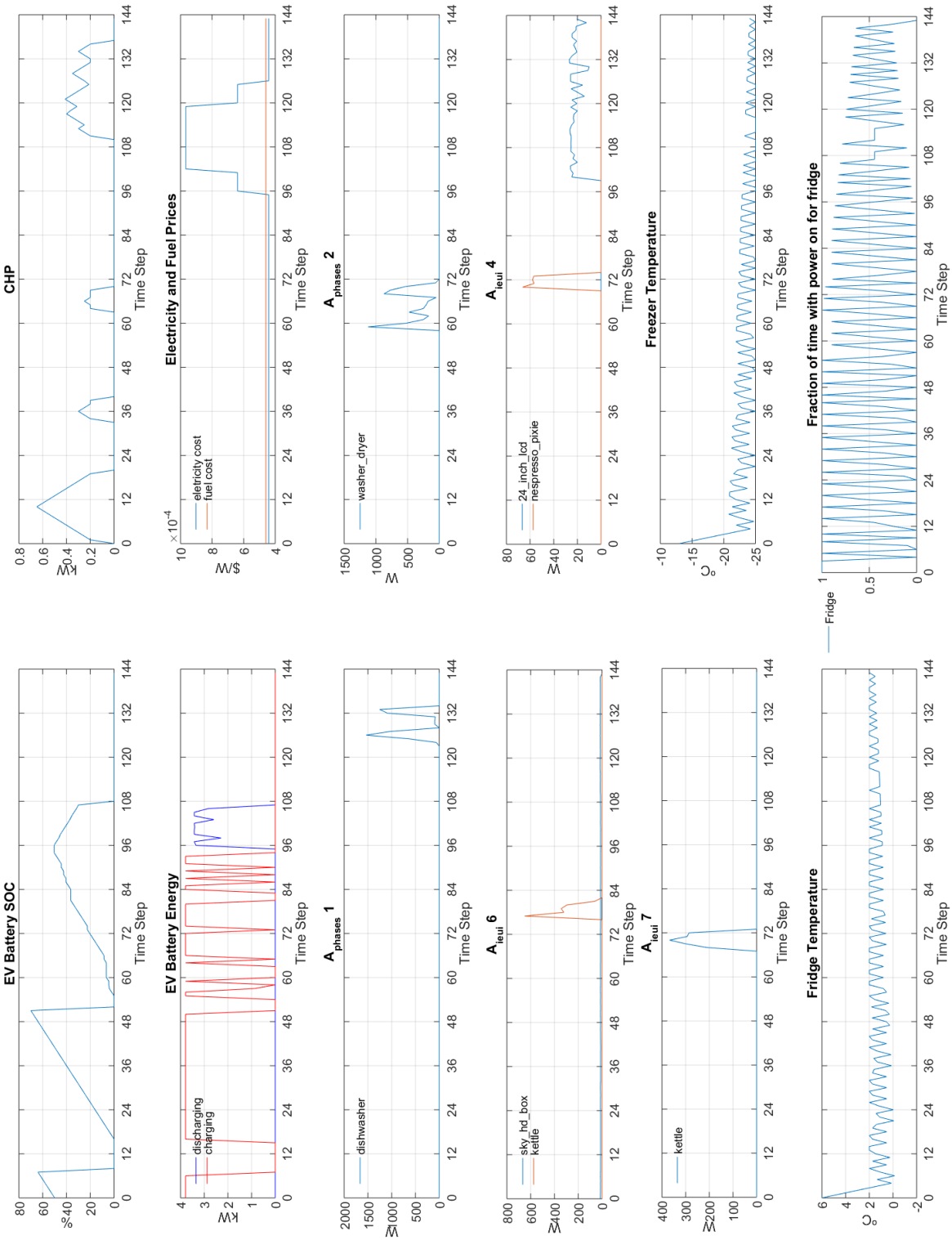

Figure 8: Results for Belo Horizonte in January.

There are 105,391 constraints and 14,886 variables. Around 30% of the variables are integers. CPLEX solved the problem in 36.64 s.

5 Conclusion

The number of smart homes is expanding worldwide. In parallel, research into HEMS is exploring how to use energy in an optimal way. One approach is to use realistic models of smart-home appliances. However, more realistic models are more difficult to solve. This work proposes a HEMS model that achieves a compromise: it is realistic but can be solved in a reasonable time. First, we proposed new fridge, shower, and EV appliance models. Then, we developed a mixed integer linear optimization model that minimizes the cost while maintaining a high level of user comfort. To illustrate the effectiveness of our model, we used real data and demonstrated that the inclusion of more details and constraints impacts the user cost. For the instances considered, our model gave results that are between 8% and 389% cheaper than those from comparable models, over a horizon of 24 hours, which corresponds to annual savings ranging from 544USD to 2205USD.

Acknowledgments

This work is supported by a full scholarship from CNPq-Brazil.

Nomenclature

Sets

A - Set of electric appliances.
$A_{IEUI} \subseteq A$ - Set of appliances with uninterruptible operation.
A^t_{IEUI} - Set of tasks from appliances $\in A_{IEUI}$.
$A^{t,a}_{IEUI} \subseteq A^t_{IEUI}$ - Set of tasks from A^t_{IEUI} of the same appliance $a \in A_{IEUI}$.
$A_{Phases} \subseteq A$ - Set of appliances with interruptible phases.
A^t_{Phases} - Set of tasks from appliances $a \in A_{Phases}$.
$A^{t,a}_{Phases} \subseteq A^t_{Phases}$ - Set of tasks from A^t_{Phases} of the same appliance $a \in A_{Phases}$.
$A^t \in \{A^t_{Phases} \cup A^t_{IEUI}\}$ - Set of appliance tasks.
B - Set of blocks in IBR.
D_{air} - Set of durations for hot or cold air needs.
D_{chu} - Set of durations for shower needs.
D_{wh} - Set of durations for hot water needs.
T - Set of time sub-intervals for scheduling horizon.
Ξ - Set of all variables.

Constants

Timing

H - Number of hours in scheduling horizon (hours).
$\Delta t_2 = H/|T|$ - Duration of each time sub-interval (hours).
$\Delta t = 60\Delta t_2$ - Duration of each time slot (minutes).
Let t be an index to represent a sub-interval of time. If we divide a horizon of $H = 24$ hours into two sub-intervals, then $\Delta t = 12$, $|T| = 2$, $t \in T = \{1, 2\}$, where $t = 1$ represents the time from 00:00h to 11:59h and $t = 2$ represents the remaining time.

Policy

E_bl^i - Energy consumption limit of block $i \in B$ (Wh).
E^t_{th} - Grid power capacity at sub-interval $t \in T$ (W).
ϖ^i - Discount to stay in block $i \in B$ (%).
λ^t - Energy consumption price at $t \in T$ (\$/Wh).
ν^t - Energy selling price at $t \in T$ (\$/Wh).

Weights

w_c - Weight factor for cost (1/\$).
w_t - Weight factor for temperature discomfort (1/°C).
w_u - Weight factor for starting time discomfort (1/h).

PV

E^t_{pv} - Power from photovoltaic panels at $t \in T$ (W).

WT

E^t_{wt} - Power from wind turbines at $t \in T$ (W).

HVAC

A_{body} - Person's body area inside home (m^2).
$A_{ceiling}$ - Area of ceiling (m^2).
A_{wall} - Area of wall (m^2).
A_{window} - Area of window (m^2).
C_{air} - Heat capacity (J/kg^{o}C).
H^t_{sun} - Solar radiation heat power at sub-interval t (W/m^2).
n_{ac} - Number of air changes (1/h).
$P^t_{activity}$ - Human activity metabolic rates at $t \in T$ (W/m^2).
P_{cool} - Rated power for air-conditioner (W).
$P_{heating}$ - Rated power for heater (W).
$R_{ceiling}$ - Heat resistance of ceiling (m^2 ^{o}C.h/J).
R_{wall} - Heat resistance of wall (m^2 ^{o}C.h/J).
R_{window} - Heat resistance of window (m^2 ^{o}C.h/J).
$SHGC$ - Solar Heat Gain Coefficient average.
T^t_f - Desired inside air temperature at $t \in T$ (^{o}C).
T^t_o - Ambient temperature at sub-interval $t \in T$ (^{o}C).
V_{house} - Volume of house (m^3).
ρ_{air} - Air density (kg/m^3).

Water Heater

$C_p = 4190 J/kg^oC$ (Thermal capacity).
E_{wh} - Binary constant, set to 1 if WH present.
fr^t_{wh} - Hot water flow rate for WH at $t \in T$ (l/m).
P_{wh} - Rated power for WH (W).
T^{wh}_f - Preferred temperature for hot water (^{o}C).
T^t_{in} - Water temperature from solar collector at $t \in T$ (^{o}C).
T^{max} - Maximal temperature for water (^{o}C).
$(UA)_{wh}$ - Loss coefficient area product for WH ($W/^oC$).
V_{tank} - Volume of water heater (WH) (dcm^3).

Shower

$C_e = 4190 J/kg^oC$ (Water specific heat).
fr^t_{chu} - Hot water flow rate for shower at $t \in T$ (l/min).
P_{chu} - Rated power for shower resistance (W).
T^{chu}_f - Preferred water temperature for shower (^{o}C).
T^t_{inlet} - Street water temperature at $t \in T$ (^{o}C).

Battery

E_{bat} - Battery capacity (kWh).
P^{ch}_{max} - Maximum charging power for battery (kW).
P^{ch}_{min} - Minimum charging power for battery (kW).
P^{dch}_{max} - Maximum discharging power for battery (kW).
P^{dch}_{min} - Minimum discharging power for battery (kW).
p_{loss} - Power float loss of battery (kW).
SOC_{max} - Maximum battery SOC without float loss (%).
SOC_{min} - Minimum battery SOC (%).
η^{ch} - Charging efficiency of inverter battery.
η^{dch} - Discharging efficiency of inverter battery.
μ - Charging/discharging efficiency of batter.

Fridge

P_{comp} - Rated power for fridge's compressor (W).
$T^{start}_{freezer}$ - Initial freezer temperature (^{o}C).
T^{start}_{refri} - Initial fridge temperature (^{o}C).
$T^{freezer}_f$ - Desired freezer temperature (^{o}C).
T^{refri}_f - Desired fridge temperature (^{o}C).

Load Profiles

D_a - Duration of task $a \in A^t_{IEUI}$ (h).
$D_{a,p}$ - Duration of phase p of task $a \in A^t_{Phases}$ (h).
DF_a - Latest finishing time for task $a \in A^t$ (h).
DS_a - Latest starting time for task $a \in A^t$ (h).
F_a - Preferred finishing time for task $a \in A^t$ (h).
P^h_a - Fixed power of task $a \in A^t_{IEUI}$ at interval h of load profile (W).
$P^h_{a,p}$ - Fixed power for phase p of task $a \in A^t_{Phases}$ at interval h of load profile (W).
PH_a - Number of phases of task $a \in A^t_{Phases}$.
S_a - Preferred starting time for task $a \in A^t$ (h).

Eletric Vehicle

$cons\_gas$ - Distance covered with one liter of fuel (km/l).
EV_{bat} - EV battery capacity (kWh).
EVP^{ch}_{max} - Maximum charging power of EV battery (kW).
EVP^{ch}_{min} - Minimum charging power of EV battery (kW).
EVP^{dch}_{max} - Maximum discharging power of EV battery (kW).
EVP^{dch}_{min} - Minimum discharging power of EV battery (kW).
EVp_{loss} - Power float loss of EV battery (kW).
$EVSOC\_last\_day$ - EV battery SOC at $t = 0$ (%).
$EVSOC_{max}$ - Maximum EV battery SOC (%).
$EVSOC_{min}$ - Minimum EV battery SOC (%).
$EVSOC^{end}_{min}$ - Minimal SOC when EV departs (%).
$EVSOC_{ret}$ - Forecast SOC when EV arrives (%).
$EV\eta^{ch}$ - Charging efficiency of inverter EV battery.
$EV\eta^{dch}$ - Discharging efficiency of inverter EV battery.
$EV\mu$ - Charging/discharging efficiency of EV battery.
km^{100} - Car autonomy with SOC at 100% (km).
Km^{s}_{next} - Distance forecast for next trip s (km).
n_{trip} - Number of complete trips in day.
$P_{gas} = \frac{price\_gas}{consu\_gas}$ - Fuel price per km traveled ($/km).
$price\_gas$ - Fuel price per liter ($/l)
t^{s}_{end} - Step time at which EV departs for trip s; it leaves at beginning of period.
t^{s}_{start} - Step time at which EV returns for trip s; it arrives at end of period.

CHP

d^{off}_{CHP} - CHP minimal time off once turned off (min).
d^{on}_{CHP} - CHP minimal time on once turned on (min).
nb^{η}_{CHP} - Number of pieces in overall piecewise efficiency function.
nb^{μ}_{CHP} - Number of pieces in piecewise efficiency function for electrical generation.
P^{ini}_{CHPe} - Initial value for variable P_{CHPe} (kW).
$P_{KW} = rate^{fuel}_{CHP} \times price\_gas$ - CHP price per kW ($/kWh).
$P^{k,\eta}_{CHP,max}\ \forall\ k = \{1..nb^{\eta}_{CHP}\}$ - Maximal power at breakpoint k in overall CHP piecewise efficiency function (kW).
$P^{k,\eta}_{CHP,min}\ \forall\ k = \{1..nb^{\eta}_{CHP}\}$ - Minimal power at breakpoint k in overall CHP piecewise efficiency function (kW).
$P^{k,\mu}_{CHP,max}\ \forall\ k = \{1..nb^{\mu}_{CHP}\}$ - Maximal power at breakpoint k in CHP piecewise efficiency function for electrical generation (kW).
$P^{k,\mu}_{CHP,min}\ \forall\ k = \{1..nb^{\mu}_{CHP}\}$ - Minimal power at breakpoint k in CHP piecewise efficiency function for electrical generation (kW).
$price^{on}_{CHP}$ - CHP start-up cost ($).
$rate^{fuel}_{CHP}$ - Fuel price per kWh for CHP (l/kWh).
r^{down}_{CHP} - Maximum ramp down for CHP (kW/min).
r^{up}_{CHP} - Maximum ramp up for CHP (kW/min).
y^{ini}_{CHP} - Initial value for variable y_{CHP}.
$y^{last\_day}_{CHP}$ - Binary, set to 1 if CHP is on at $t = 0$.
$\bar{\eta}$ - Overall efficiency average.
$\eta^{k}_{CHP,p}\ \forall\ k = \{1..nb^{\eta}_{CHP}\}$ - Image at breakpoint k in overall CHP piecewise efficiency function (%).
$\bar{\mu}$ - Electrical generation efficiency average.
$\mu^{k}_{CHP,p}\ \forall\ k = \{1..nb^{\mu}_{CHP}\}$ - Image at breakpoint k in CHP piecewise efficiency function for electrical generation (%).

Variables

Discomfort

U^{t}_{a} - Time discomfort due to deviation from target for appliance a at $t \in T$ (h).
V^{t}_{a} - Temperature discomfort due to deviation from target temperature of appliance a at $t \in T$ (^{o}C).
ζ_a - Discomfort for not doing task $a \in A^{t}_{IEUI}$ (h).
$\Psi_{a,p}$ - Discomfort for not doing phase p of task $a \in A^{t}_{Phases}$ (h).

HVAC

T^{t}_{room} - Room temperature at sub-interval $t \in T$ (^{o}C).
y^{t}_{air} - On/off binary for air-conditioner operation at $t \in T$.
y^{t}_{HVAC} - On/off binary for heating operation at $t \in T$.
z^{t}_{air} - Fraction of Δ_t in $t \in T$ during which air-conditioner is on.
z^{t}_{HVAC} - Fraction of Δ_t in $t \in T$ during which heating is on.

WH

$T^t_{out,wh}$ - Water heater output temperature at $t \in T$ (^{o}C).
y^t_{wh} - On/off binary for water heater operation at $t \in T$.

Shower

$T^t_{chu\_hand}$ - Shower water temperature manually adjusted at sub-interval t (^{o}C).
$T^t_{out,chu}$ - Shower output water temperature at $t \in T$ (^{o}C).
$y^t_{chu,hot}$ - On/off binary for shower operation at $t \in T$.

Battery

$P^{ch,t}_{bat}$ - Charging power of battery (kW).
$P^{dch,t}_{bat}$ - Discharging power of battery (kW).
SOC^t - Battery's state of charge at sub-interval t (%).
$y^{ch,t}_{bat}$ - On/off binary for battery charging at $t \in T$.
$y^{dch,t}_{bat}$ - On/off binary for battery discharging at $t \in T$.
y^t_{float} - Binary to activate battery float losses at $t \in T$.

Fridge

$T^t_{freezer}$ - Freezer temperature at sub-interval t (^{o}C).
T^t_{refri} - Fridge temperature at sub-interval t (^{o}C).
y^t_{comp} - On/off binary for fridge's compressor at $t \in T$.

Eletric Vehicle

C_{ev} - Fuel cost used in electric vehicle (EV) ($).
C^s_{ev} - Cost related to fuel used in trip s ($).
$EVSOC^t$ - EV battery's state of charge at $t \in T$ (%).
Km^s_{fuel} - Number of km for trip s using fuel (km).
$P^{ch,t}_{EVbat}$ - Charging power of EV battery (kW).
$P^{dch,t}_{EVbat}$ - Discharging power of EV battery (kW).
$y^{ch,t}_{EVbat}$ - On/off binary for EV battery charging at $t \in T$.
$y^{dch,t}_{EVbat}$ - On/off binary for EV battery discharging at $t \in T$.
$y^t_{EVfloat}$ - Binary to start EV battery float losses at $t \in T$.

CHP

C^t_{CHP} - CHP cost operation at sub-interval $t \in T$ ($).
P^t_{CHPe} - CHP electrical power output at $t \in T$ (KW).
$P^t_{CHP,fuel}$ - CHP power input from fuel at $t \in T$ (KW).
P^t_{CHPt} - CHP thermal power output at $t \in T$ (KW).
w^t_{down} - Fraction of Δ_t in $t \in T$ in which CHP ramps down.
w^t_{up} - Fraction of Δ_t in $t \in T$ in which CHP ramps up.
y^t_{CHP} - On/off binary for CHP operation at $t \in T$.
z^t_{CHP} - Binary to determine if CHP is turned on at $t \in T$.
zd^t_{CHP} - Binary to determine if CHP is turned off at $t \in T$.

A^t_{IEUI}

y^t_a - Binary that indicates whether or not operation of task $a \in A^t_{IEUI}$ starts at sub-interval t.
$y_{a,b}$ - Binary that indicates if task $a \in A^t_{IEUI}$ has to be done after task $b \in A^t_{IEUI}$ is finished.

A^t_{Phases}

$y^t_{a,p}$ - Binary that indicates if phase p of task $a \in A^t_{Phases}$ starts at sub-interval t.
$y^p_{a,b}$ - Binary that indicates if task $a \in A^t_{Phases}$ has to be done after task $b \in A^t_{Phases}$ is finished.

Other

C^t - Monetary cost at $t \in T$ ($).
E^t_{av} - Fixed power credit available at $t \in T$ (W).
E^t_g - Fixed power taken from grid at $t \in T$ (W).
$E^{t,i}_g$ - Fixed power taken from grid at $t \in T$ for block $i \in B$ (W).
E^t_v - Fixed power injected into grid at $t \in T$ (W).
x^t_a - Fixed power consumption of appliance a at $t \in T$(W).
y^i_g - Binary to determine whether or not block $i \in B$ is selected.

References

[1] Mahmoud Abdelhamid, Srikanth Pilla, Rajendra Singh, Imtiaz Haque, and Zoran Filipi. A comprehensive optimized model for on-board solar photovoltaic system for plug-in electric vehicles: energy and economic impacts. International Journal of Energy Research, 40(11):1489–1508, 2016.

[2] Christopher O. Adika and Lingfeng Wang. Autonomous appliance scheduling for household energy management. IEEE Transactions on Smart Grid, 5(2):673–682, 2014.

[3] Christopher O. Adika and Lingfeng Wang. Smart charging and appliance scheduling approaches to demand side management. International Journal of Electrical Power & Energy Systems, 57:232–240, 2014.

[4] Alessandro Agnetis, Gianluca de Pascale, Paolo Detti, and Antonio Vicino. Load scheduling for household energy consumption optimization. IEEE Transactions on Smart Grid, 4(4):2364–2373, 2013.

[5] Refrigerating American Society of Heating and Inc. Air-Conditioning Engineers. 2013 ASHRAE Handbook - Fundamentals (SI Edition). ASHRAE, 2013.

[6] Refrigerating American Society of Heating and Inc. Air-Conditioning Engineers. 2015 ASHRAE HANDBOOK Heating, Ventilating, and Air-Conditioning APPLICATIONS (SI Edition). ASHRAE, 2015.

[7] ANEEL. Matriz de energia eltrica. accessed Dec. 2017.

[8] Amjad Anvari-Moghaddam, Hassan Monsef, and Ashkan Rahimi-Kian. Cost-effective and comfort-aware residential energy management under different pricing schemes and weather conditions. Energy and Buildings, 86:782–793, 2015.

[9] Amjad Anvari-Moghaddam, Hassan Monsef, and Ashkan Rahimi-Kian. Optimal smart home energy management considering energy saving and a comfortable lifestyle. IEEE Transactions on Smart Grid, 6(1):324–332, 2015.

[10] A. Arabali, M. Ghofrani, M. Etezadi-Amoli, M. S. Fadali, and Y. Baghzouz. Genetic-algorithm-based optimization approach for energy management. IEEE Transactions on Power Delivery, 28(1):162–170, 2013.

[11] Sean Barker, Sandeep Kalra, David Irwin, and Prashant Shenoy. Empirical characterization and modeling of electrical loads in smart homes. 2013 International Green Computing Conference (IGCC), pages 1–10, 2013.

[12] Marc Beaudin and Hamidreza Zareipour. Home energy management systems: A review of modelling and complexity. Renewable and Sustainable Energy Reviews, 45:318–335, 2015.

[13] Bruno N. Borges. Modelagem semi-emprica de um refrigerador frost-free sujeito a abertura de portas. 2013. Thesis, Universidade Federal de Santa Catarina, Florianpolis, 2013.

[14] Bruno N. Borges, Christian J. L. Hermes, Joaquim M. Gonalves, and Cludio Melo. Transient simulation of household refrigerators: A semi-empirical quasi-steady approach. Applied Energy, 88(3):748–754, 2011.

[15] Brazil. Lei n 12.212, de 20 de janeiro de 2010, 2010. accessed Dec. 2017.

[16] M. Castillo-Cagigal, E. Caamao-Martn, E. Matallanas, D. Masa-Bote, A. Gutirrez, F. Monasterio-Huelin, and J. Jimnez-Leube. PV self-consumption optimization with storage and active DSM for the residential sector. Solar Energy, 85(9):2338–2348, 2011.

[17] Cemig. Cities of the future project. accessed Dec. 2017.

[18] Chen Chen, Jianhui Wang, Yeonsook Heo, and Shalinee Kishore. MPC-based appliance scheduling for residential building energy management controller. IEEE Transactions on Smart Grid, 4(3):1401–1410, 2013.

[19] Xiaodao Chen, Tongquan Wei, and Shiyan Hu. Uncertainty-aware household appliance scheduling considering dynamic electricity pricing in smart home. IEEE Transactions on Smart Grid, 4(2):932–941, 2013.

[20] Zhi Chen, Lei Wu, and Yong Fu. Real-time price-based demand response management for residential appliances via stochastic optimization and robust optimization. IEEE Transactions on Smart Grid, 3(4):1822–1831, 2012.

[21] Nicos Christofides, R. Alvarez-Valdes, and J. M. Tamarit. Project scheduling with resource constraints: A branch and bound approach. European Journal of Operational Research, 29(3):262–273, 1987.

[22] Gregory Chagas da Costa Gomes. Avaliao do comportamento de refrigeradores domsticos frente a defeitos provocados e emulados. Thesis, Universidade Federal de Santa Catarina, 2015.

[23] Alessandro Jos da Silva, Carlos Roberto Costa Nascimento, Leandro Ferreira da Silva, and Taza de Pinho Barroso Lucas. Anlise topoclimtica em unidade de conservao urbana a partir da temperatura e umidade relativa do ar. e-Scientia, 4(1):21–30, 2011.

[24] Michel De Lara, Pierre Carpentier, Jean-Philippe Chancelier, and Vincent Leclere. Optimization methods for the smart grid. Report commissioned by the Conseil Franais de lEnergie, Ecole des Ponts ParisTech, 2014.

[25] W. De Soto, S. A. Klein, and W. A. Beckman. Improvement and validation of a model for photovoltaic array performance. Solar Energy, 80(1):78–88, 2006.

[26] Ruilong Deng, Zaiyue Yang, Jiming Chen, and Mo-Yuen Chow. Load scheduling with price uncertainty and temporally-coupled constraints in smart grids. IEEE Transactions on Power Systems, 29(6):2823–2834, 2014.

[27] William B. DeOreo, Peter W. Mayer, Benedykt Dziegielewski, and Jack Kiefer. Residential end uses of water, version 2. Water Research Foundation, 2016.

[28] Katia Gregio Di Santo, Eduardo Kanashiro, Silvio Giuseppe Di Santo, and Marco Antonio Saidel. A review on smart grids and experiences in brazil. Renewable and Sustainable Energy Reviews, 52:1072–1082, 2015.

[29] Pengwei Du and Ning Lu. Appliance commitment for household load scheduling. IEEE Transactions on Smart Grid, 2(2):411–419, 2011.

[30] John A Duffie and William A Beckman. Solar Engineering of Thermal Processes, volume 4. Wiley New York, 2013.

[31] Mohamed E. El-hawary. The smart gridstate-of-the-art and future trends. Electric Power Components and Systems, 42(3–4):239–250, 2014.

[32] Energtica, Empresa de Pesquisa. Plano Nacional de Energia 2030. EPE, Rio de Janeiro, 2007.

[33] Ozan Erdinc, Nikolaos G. Paterakis, Tiago D. P. Mendes, Anastasios G. Bakirtzis, and Joao P. S. Catalao. Smart household operation considering bi-directional EV and ESS utilization by real-time pricing-based DR. IEEE Transactions on Smart Grid, 6(3):1281–1291, 2015.

[34] M. Erol-Kantarci and H. T. Mouftah. Wireless sensor networks for cost-efficient residential energy management in the smart grid. IEEE Transactions on Smart Grid, 2(2):314–325, 2011.

[35] M. Fadaeenejad, A. M. Saberian, Mohd Fadaee, M. A. M. Radzi, H. Hizam, and M. Z. A. AbKadir. The present and future of smart power grid in developing countries. Renewable and Sustainable Energy Reviews, 29:828–834, 2014.

[36] Mohammad Ali Fotouhi Ghazvini, Joo Soares, Omid Abrishambaf, Rui Castro, and Zita Vale. Demand response implementation in smart households. Energy and Buildings, 143:129–148, 2017.

[37] Sajjad Golshannavaz. Cooperation of electric vehicle and energy storage in reactive power compensation: An optimal home energy management system considering PV presence. Sustainable Cities and Society, 39:317–325, 2018.

[38] Sebastian Gottwalt, Wolfgang Ketter, Carsten Block, John Collins, and Christof Weinhardt. Demand side managementA simulation of household behavior under variable prices. Energy Policy, 39(12):8163–8174, 2011.

[39] A. D. Hawkes, D. J. L. Brett, and N. P. Brandon. Fuel cell micro-CHP techno-economics: Part 1 Model concept and formulation. International Journal of Hydrogen Energy, 34(23):9545–9557, 2009.

[40] A. D. Hawkes, D. J. L. Brett, and N. P. Brandon. Fuel cell micro-CHP techno-economics: Part 2 Model application to consider the economic and environmental impact of stack degradation. International Journal of Hydrogen Energy, 34(23):9558–9569, 2009.

[41] Ying-Yi Hong, Jie-Kai Lin, Ching-Ping Wu, and Chi-Cheng Chuang. Multi-objective air-conditioning control considering fuzzy parameters using immune clonal selection programming. IEEE Transactions on Smart Grid, 3(4):1603–1610, 2012.

[42] Tanguy Hubert and Santiago Grijalva. Modeling for residential electricity optimization in dynamic pricing environments. IEEE Transactions on Smart Grid, 3(4):2224–2231, 2012.

[43] Jony Javorski Eckert, Ludmila Corra de Alkmin e Silva, Fabio Mazzariol Santiciolli, Eduardo dos Santos Costa, Fernanda Cristina Corra, and Franco Giuseppe Dedini. Energy storage and control optimization for an electric vehicle. International Journal of Energy Research, 42(11):3506–3523, 2018.

[44] Anders Frick Johan Fagerberg. Smart homes and home automation. Technical report, Berg Insight, 2015.

[45] Jack Kelly and William Knottenbelt. The UK-DALE dataset, domestic appliance-level electricity demand and whole-house demand from five UK homes. Scientific Data, 2:150007, 2015.

[46] Muhammad Asghar Khan, Nadeem Javaid, Anzar Mahmood, Zahoor Ali Khan, and Nabil Alrajeh. A generic demand-side management model for smart grid. International Journal of Energy Research, 39(7):954–964, 2015.

[47] Tng T. Kim and H. Vincent Poor. Scheduling power consumption with price uncertainty. IEEE Transactions on Smart Grid, 2(3):519–527, 2011.

[48] Phillip Oliver Kriett and Matteo Salani. Optimal control of a residential microgrid. Energy, 42(1):321–330, 2012.

[49] Jang-Won Lee and Du-Han Lee. Residential electricity load scheduling for multi-class appliances with time-of-use pricing. IEEE International Workshop on Smart Grid Communications and Networks, pages 1194–1198., 2011.

[50] Andra P. Leite, Djalma M. Falco, and Carmen L.T. Borges. Modelagem de usinas elicas para estudos de confiabilidade. Sba: Controle & Automao Sociedade Brasileira de Automatica, 17:177–188, 2006.

[51] Benot Lvesque, Michel Lavoie, and Jean Joly. Residential water heater temperature: 49 or 60 degrees celsius? The Canadian Journal of Infectious Diseases, 15(1):11–12, 2004.

[52] F. Y. Melhem, O. Grunder, Z. Hammoudan, and N. Moubayed. Optimization and energy management in smart home considering photovoltaic, wind, and battery storage system with integration of electric vehicles. Canadian Journal of Electrical and Computer Engineering-Revue Canadienne De Genie Electrique Et Informatique, 40(2):128–138, 2017.

[53] Henrique Leo de S Menezes. Avaliao da aplicao da modalidade tarifria horria branca: Estudo de caso para consumidores residenciais. Report, Universidade de Braslia, 2015.

[54] Ministrio de Minas e Energia. Projeo da demanda de energia eltrica para os prximos 5 anos (2016-2020), volume NOTA TCNICA DEA 19/15. EPE, 2015.

[55] Amin Mohseni, Seyed Saeidollah Mortazavi, Ahmad Ghasemi, Ali Nahavandi, and Masoud Talaei abdi. The application of household appliances' flexibility by set of sequential uninterruptible energy phases model in the day-ahead planning of a residential microgrid. Energy, 139:315–328, 2017.

[56] Amir-Hamed Mohsenian-Rad and Alberto Leon-Garcia. Optimal residential load control with price prediction in real-time electricity pricing environments. IEEE Transactions on Smart Grid, 1(2):120–133, 2010.

[57] Chukwuka G. Monyei, Aderemi O. Adewumi, Daniel Akinyele, Olubayo M. Babatunde, Michael O. Obolo, and Joshua C. Onunwor. A biased load manager home energy management system for low-cost residential building low-income occupants. Energy, 150:822–838, 2018.

[58] Afshin Najafi-Ghalelou, Sayyad Nojavan, and Kazem Zare. Heating and power hub models for robust performance of smart building using information gap decision theory. International Journal of Electrical Power & Energy Systems, 98:23–35, 2018.

[59] Duong Tung Nguyen and Long Bao Le. Joint optimization of electric vehicle and home energy scheduling considering user comfort preference. IEEE Transactions on Smart Grid, 5(1):188–199, 2014.

[60] Hieu T Nguyen, Duong T Nguyen, and Long B Le. Energy management for households with solar assisted thermal load considering renewable energy and price uncertainty. IEEE Transactions on Smart Grid, 6(1):301–314, 2015.

[61] Xuan Hieu Nguyen and Minh Phuong Nguyen. Mathematical modeling of photovoltaic cell/module/arrays with tags in Matlab/Simulink. Environmental Systems Research, 4(1), 2015.

[62] NISSAN. Nissan Leaf presentation. accessed Dec. 2017.

[63] Nikolaos G. Paterakis, Ozan Erdinc, Anastasios G. Bakirtzis, and Joao P. S. Catalao. Optimal household appliances scheduling under day-ahead pricing and load-shaping demand response strategies. IEEE Transactions on Industrial Informatics, 11(6):1509–1519, 2015.

[64] Michael Angelo A. Pedrasa, Ted D. Spooner, and Iain F. MacGill. Coordinated scheduling of residential distributed energy resources to optimize smart home energy services. IEEE Transactions on Smart Grid, 1(2):134–143, 2010.

[65] Michael Angelo A. Pedrasa, Ted D. Spooner, and Iain F. MacGill. A novel energy service model and optimal scheduling algorithm for residential distributed energy resources. Electric Power Systems Research, 81(12):2155–2163, 2011.

[66] Manisa Pipattanasomporn, Murat Kuzlu, Saifur Rahman, and Yonael Teklu. Load profiles of selected major household appliances and their demand response opportunities. IEEE Transactions on Smart Grid, 5(2):742–750, 2014.

[67] Li Ping Qian, Ying Jun Angela Zhang, Jianwei Huang, and Yuan Wu. Demand response management via real-time electricity price control in smart grids. IEEE Journal on Selected Areas in Communications, 31(7):1268–1280, 2013.

[68] Mohammad Rastegar, Mahmud Fotuhi-Firuzabad, and Farrokh Aminifar. Load commitment in a smart home. Applied Energy, 96:45–54, 2012.

[69] Ian Richardson, Murray Thomson, David Infield, and Conor Clifford. Domestic electricity use: A high-resolution energy demand model. Energy and Buildings, 42(10):1878–1887, 2010.

[70] E. M. G. Rodrigues, R. Godina, E. Pouresmaeil, J. R. Ferreira, and J. P. S. Catalo. Domestic appliances energy optimization with model predictive control. Energy Conversion and Management, 142:402–413, 2017.

[71] Hee-Tae Roh and Jang-Won Lee. Residential demand response scheduling with multiclass appliances in the smart grid. IEEE Transactions on Smart Grid, 7(1):94–104, 2016.

[72] Ameena Saad al sumaiti, Mohammed Hassan Ahmed, and Magdy M. A. Salama. Smart home activities: A literature review. Electric Power Components and Systems, 42(3–4):294–305, 2014.

[73] Miadreza Shafie-Khah and Pierluigi Siano. A stochastic home energy management system considering satisfaction cost and response fatigue. IEEE Transactions on Industrial Informatics, 14(2):629–638, 2018.

[74] Mohammad Shakeri, Mohsen Shayestegan, Hamza Abunima, S. M. Salim Reza, M. Akhtaruzzaman, A. R. M. Alamoud, Kamaruzzaman Sopian, and Nowshad Amin. An intelligent system architecture in home energy management systems (HEMS) for efficient demand response in smart grid. Energy and Buildings, 138:154–164, 2017.

[75] Shengnan Shao, Manisa Pipattanasomporn, and Saifur Rahman. Development of physical-based demand response-enabled residential load models. IEEE Transactions on Power Systems, 28(2):607–614, 2013.

[76] Elham Shirazi and Shahram Jadid. Cost reduction and peak shaving through domestic load shifting and DERs. Energy, 124:146–159, 2017.

[77] Elham Shirazi, Alireza Zakariazadeh, and Shahram Jadid. Optimal joint scheduling of electrical and thermal appliances in a smart home environment. Energy Conversion and Management, 106:181–193, 2015.

[78] Javier Silvente and Lazaros G. Papageorgiou. An MILP formulation for the optimal management of microgrids with task interruptions. Applied Energy, 206:1131–1146, 2017.

[79] Alireza SoltaniNejad Farsangi, Shahrzad Hadayeghparast, Mehdi Mehdinejad, and Heidarali Shayanfar. A novel stochastic energy management of a microgrid with various types of distributed energy resources in presence of demand response programs. Energy, 160:257–274, 2018.

[80] T. Sousa, H. Morais, Z. Vale, P. Faria, and J. Soares. Intelligent energy resource management considering vehicle-to-grid: A simulated annealing approach. IEEE Transactions on Smart Grid, 3(1):535–542, 2012.

[81] L. Stankovic, V. Stankovic, J. Liao, and C. Wilson. Measuring the energy intensity of domestic activities from smart meter data. Applied Energy, 183:1565–1580, 2016.

[82] Roland Stull. Practical Meteorology: An Algebra Based Survey of Atmospheric Science. BC Campus, 2016.

[83] Dimitrios Thomas, Olivier Deblecker, and Christos S. Ioakimidis. Optimal operation of an energy management system for a grid-connected smart building considering photovoltaics uncertainty and stochastic electric vehicles driving schedule. Applied Energy, 210:1188–1206, 2018.

[84] George Tsagarakis, Adam Collin, and Aristides Kiprakis. A statistical survey of the UK residential sector electrical loads. International Journal of Emerging Electric Power Systems, 14(5), 2013.

[85] D. Villanueva and A. Feijo. Wind power distributions: A review of their applications. Renewable and Sustainable Energy Reviews, 14(5):1490–1495, 2010.

[86] Chengshan Wang, Yue Zhou, Bingqi Jiao, Yamin Wang, Wenjian Liu, and Dan Wang. Robust optimization for load scheduling of a smart home with photovoltaic system. Energy Conversion and Management, 102:247–257, 2015.

[87] Zaiyue Yang, Keyu Long, Pengcheng You, and Mo-Yuen Chow. Joint scheduling of large-scale appliances and batteries via distributed mixed optimization. IEEE Transactions on Power Systems, 30(4):2031–2040, 2015.

[88] Wen Yao-Jung and Alice M. Agogino. Wireless networked lighting systems for optimizing energy savings and user satisfaction. Proceedings of Wireless Hive Networks Conference, pages 1–7, 2008.

[89] Zhe Yu, Liyan Jia, Mary C. Murphy-Hoye, Annabelle Pratt, and Lang Tong. Modeling and stochastic control for home energy management. IEEE Transactions on Smart Grid, 4(4):2244–2255, 2013.

[90] A Cengel Yunus. Heat Transfer: A Practical Approach. McGraw-Hill, New York, 2003.

[91] Heng Zhang, Haiping Chen, Haowen Liu, Jiguang Huang, Xinxin Guo, and Mingjie Li. Design and performance study of a low concentration photovoltaic-thermal module. International Journal of Energy Research, 42(6):2199–2212, 2018.

[92] Bin Zhou, Wentao Li, Ka Wing Chan, Yijia Cao, Yonghong Kuang, Xi Liu, and Xiong Wang. Smart home energy management systems: Concept, configurations, and scheduling strategies. Renewable and Sustainable Energy Reviews, 61:30–40, 2016.

[93] Suyang Zhou, Zhi Wu, Jianing Li, and Xiao-ping Zhang. Real-time energy control approach for smart home energy management system. Electric Power Components and Systems, 42(3–4):315–326, 2014.

[94] Zhao Zhuang, Lee Won Cheol, Shin Yoan, and Song Kyung-Bin. An optimal power scheduling method for demand response in home energy management system. IEEE Transactions on Smart Grid, 4(3):1391–1400, 2013.